의학석사 학위논문

Mechanism of Extracellular Aggregate-induced Alpha-synuclein Transmission

세포 외 응집체에 의해 유도된 알파-시뉴클린 전이 매커니즘

2018 년 2 월

서울대학교 대학원

의과대학 의과학과

임 윤 주

Mechanism of Extracellular Aggregate-induced Alpha-synuclein Transmission

지도 교수 이 승 재

이 논문을 의학석사 학위논문으로 제출함

2017 년 10 월

서울대학교 대학원

의과대학 의과학과

임 윤 주

임윤주의 의학석사 학위논문을 인준함

2018 년 1 월

위 원 장 묵 인희 (인)

부위원장 이 승재 (인)

위 원 서 영호 (인)

Mechanism of Extracellular Aggregate-induced Alpha-synuclein Transmission

by

Yoon-Ju Lim

A thesis submitted to the Department of Biomedical Science in partial fulfillment of the requirements for the Degree of Master of Science in Biomedical Science at Seoul National University College of Medicine

January 2018

Approved by Thesis Committee:

Professor Inhee Mook-Jung Chairman

Professor Seung-Jae Lee Vice chairman

Professor Young Ho Suh

ABSTRACT

Mechanism of Extracellular Aggregate-induced Alpha-synuclein Transmission

Yoon-Ju Lim

Department of Biomedical Science

The Graduate School

Seoul National University

Deposition of alpha-synuclein (αSyn) aggregates is a pathological feature of Parkinson's disease. Cell-to-cell transmission of αSyn aggregates was suggested as the underlying mechanism of the progression of Parkinson's disease. According to the 'prion-like' spreading hypothesis, aggregate transmission increases dependently on the template seeding mechanism. αSyn aggregates work like infectious prion, amplifying protein aggregation and accumulation. However, this still remains unclear. V40G variant of αSyn has seeding blocking property; thereby elucidation of template seeding hypothesis becomes possible. Here, αSyn aggregate transmission rate was observed using Bimolecular Fluorescence Complementation (BiFC) system to verify whether this seeding ability plays a major role in αSyn aggregate propagation. Aggregate transmission level was increased in the V40G aggregate treated condition

even the V40G aggregate has no seeding activity. Therefore, αSyn aggregate transmission might involve the mechanism other than the direct template seeding. To elucidate the mechanism of transmission, I assessed the endo-lysosomal degradation rate using fluorescein-conjugated dextran. When the cells were exposed to the extracellular αSyn, the endo-lysosomal degradation rate was decreased, while the lysosomal integrity and function were unaffected. RNA sequencing analysis revealed that the pathways related to the transcriptional regulation, cytoskeleton organization, immune response, and mitochondria were changed by extracellular αSyn aggregates. Altogether, this study suggests that the templated seeding mechanism is not the main principle of αSyn aggregate propagation and that the mechanism is related with the changes in the trafficking through the endo-lysosomal pathway.

Keywords: Parkinson's disease, Cell-to-cell transmission, Protein aggregates, Alpha-synuclein, Endo-lysosomal pathway, Transcriptomics, Gene expression change

Student Number: 2016-22004

CONTENTS

LIST OF FIGURES

LIST OF TABLES

LIST OF ABBREVIATIONS

ARSA : Arylsulfatase A

αSyn : alpha-synuclein

BafA1 : Bafilomycin A1

BiFC : Bimolecular Fluorescence Complementation

CD : Circular dichroism spectroscopy

CRD : Carbohydrate-recognition-binding domain

CTSD : Cathepsin D

DAn : Dopaminergic neurons

DEG : Database of essential genes

DLB : Dementia with Lewy bodies

ER : Endoplasmic reticulum

FC : Fold change

GBA : Glucocerebrosidase; Gcase

Hsp70 : Heat shock protein 70

iPSC : Induced pluripotent stem cell

LAMP2 : Lysosome-associated membrane protein 2

LBs : Lewy bodies

LMP : Lysosomal membrane permeabilization

LNs : Lewy neurites

LPS : Lipopolysaccharides

MHC II : Major histocompatibility complex II

MSA : Multiple system atrophy

NAC : non-amyloid β component

PBS : Phosphate-buffered saline

PD : Parkinson’s disease

PDI : Protein disulfide-isomerase

RNA-seq : Quant mRNA Sequencing

SGII : Secretogranin II

SV2 : αSyn-Venus2

ThT : Thioflavin T

Tx : Triton-X 100

V1S : Venus1-αSyn

WT : Wild type

INTRODUCTION

Clinical and pathological features of Parkinson's disease

Parkinson's disease (PD), the second most common neurodegenerative disease, is characterized by dopaminergic neuron loss in the substantia nigra pars compacta [1]. This causes several movement disorders such as rigidity, resting tremor, balance impairment, and bradykinesia [1]. PD is one of the synucleinopathies, a group of diseases which includes multiple system atrophy (MSA) and dementia with Lewy bodies (DLB), and has pathological feature of α-synuclein (αSyn) aggregate deposition in the central and peripheral nervous systems [2-5]. Those αSyn aggregates, in the forms of Lewy bodies (LBs) and Lewy neurites (LNs), spread into larger area of the brain as the disease progresses [6-8]. As αSyn aggregates in the brain spread gradually, more progressive disease symptoms appear [7]. Amyloid fibril form of αSyn, enriched in the cross β-sheet conformations, is the most abundant component of LBs [9, 10]. Endogenous αSyn level increases by duplication or triplication of αSyn gene and it causes forms of PD [11-13]. αSyn overexpression replicates pathological symptoms of PD and other synucleinopathies such as typical neuropathologic inclusions and neuronal degradation concomitant with motor symptoms in transgenic animal models [14].

Cell-to-cell transmission of αSyn aggregates in Parkinson's disease

In early stage of PD, αSyn aggregates appear in the low brain stem and those aggregates spread gradually into the midbrain and neocortical areas [1]. This pathological propagation of aggregates can be explained by the mechanism called 'cell-to-cell transmission' [6, 15, 16]. Evidence for the cell-to-cell transmission of αSyn aggregates in progression of PD has been growing for the past several years [16-19]. Mechanism of the transmission has not been fully understood. For the propagation of intracellular aggregated proteins, they were secreted from neurons [6]. αSyn aggregates were secreted through an unconventional secretory pathway, or endoplasmic reticulum (ER)/Golgi-independent pathway [20, 21]. When those secreted aggregates transferred to other cells, they might lead to progressive propagation of cellular pathology.

There is a 'prion-like' spreading hypothesis for protein aggregate transmission in neurodegenerative diseases. The fibrils can form spontaneously and follow nucleation-dependent process which has a long lag phase and then an exponential growth phase (Figure 1A) [22]. Addition of pre-formed aggregates dramatically reduces the lag phase of the nucleation-dependent fibrillation thereby aggregates are produced rapidly [17]. This is a seeded conformational-templating molecular principle, underlying the infectious and transmissible characteristics of prion and pre-formed aggregates work as 'seed' like infectious prion [8, 23]. Pathology of diseases propagates from a few separate regions to other regions in a prion-like manner [8, 17, 23, 24], according to the stereotypical progress stages described by Braak [25]. Up till now, it has been thought that protein aggregate transmission depends on the seeded conformational-templating (Figure 1B). However, it has not been completely proven whether the increase of aggregate transmission is because

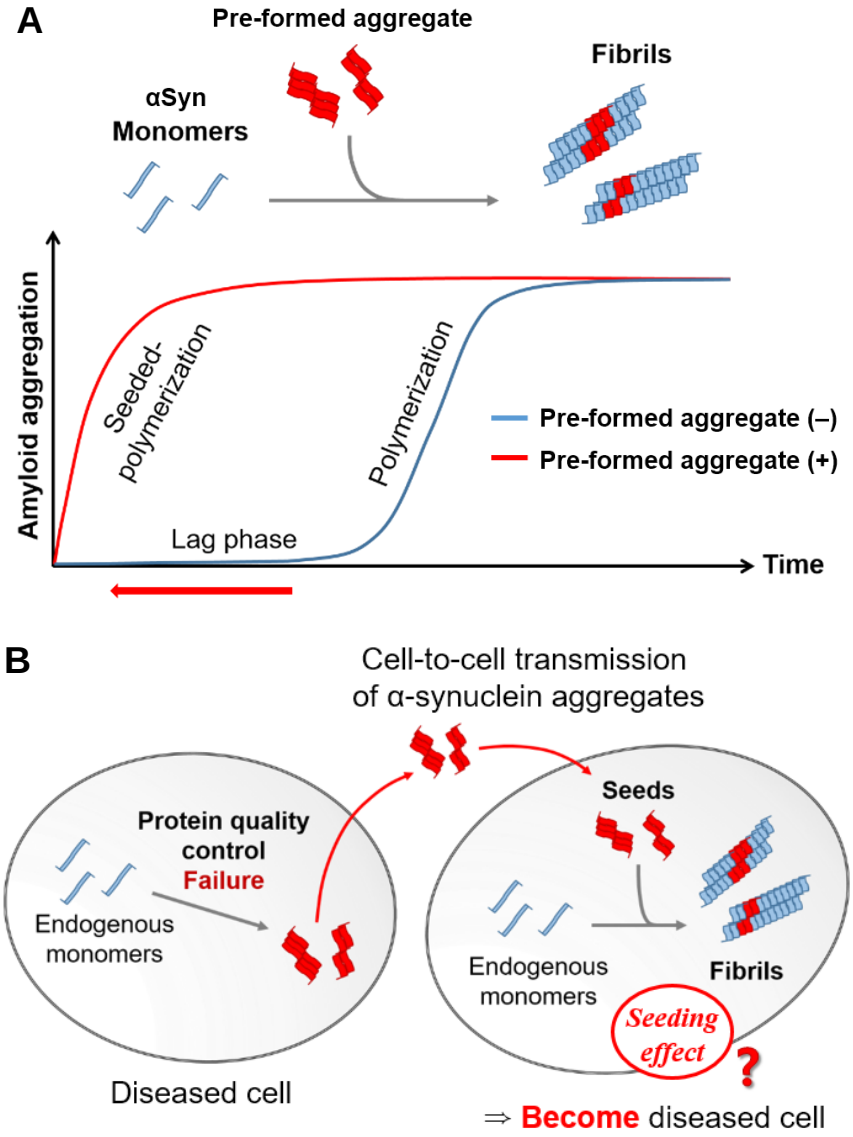

Figure 1. Kinetic principle of protein aggregation underlying the intercellular aggregate transmission

(A) Simplified scheme of the protein fibrillation kinetics and seeded polymerization.

(B) Illustration of seeded polymerization in cell-to-cell aggregate transmission.

of this seeding-dependent mechanism. By doing so, studies to elucidate the effect of seeding-dependent mechanism in aggregate transmission progress are needed.

Structure of αSyn

αSyn is a natively unfolded protein of 140 amino acids, concentrated at the presynaptic terminals in neurons (Figure 2A) [26]. The N-terminus of αSyn consists of an amphipathic region (1-60 aa), a hydrophobic non-amyloid β component (NAC) region in the center (61-95 aa), and the C-terminus of αSyn consists of a highly acidic region (96-140 aa) [27, 28]. The NAC region plays a crucial role in protein aggregation [29]. When αSyn binds to the cellular membrane, αSyn changes its form to α-helix structures (Figure 2B, C) [29]. There are two helix structures on both sides of the linker part (38-44 aa). And this structural flexibility of the linker region might have a profound influence in the aggregation propensity of αSyn.

Characteristics of V40G variant of αSyn

In the previous study [30], recombinant mutant V40G αSyn, changed valine to glycine in the linker part of αSyn, was made which expected to have a structure preventing αSyn fibrillation. To characterize recombinant WT and V40G mutant αSyn, fibrillation, circular dichroism (CD) spectroscopy and seeded fibrillation were conducted. αSyn monomers were enriched in β-sheet conformation and formed

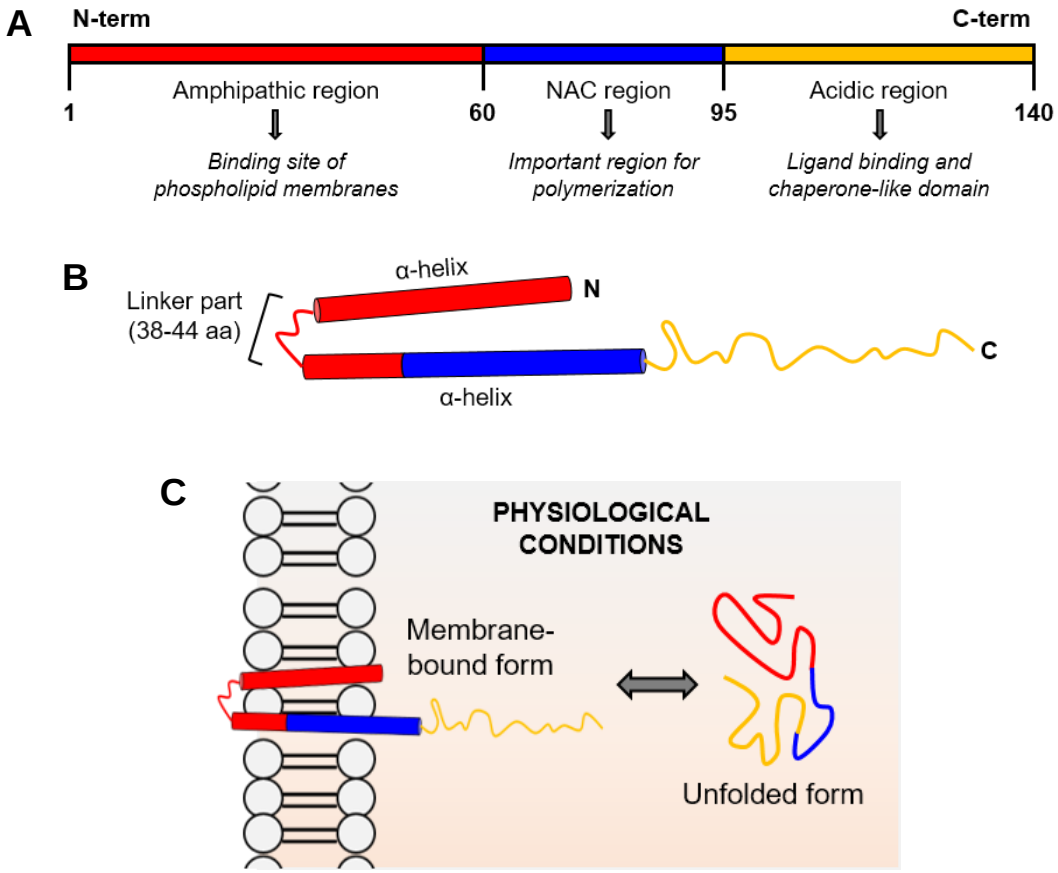

Figure 2. Structures of αSyn

(A) Schematic illustration of the primary structure of αSyn. The 140 amino acid chain consists of three major regions. (B) Secondary structure of αSyn. Two α-helical structures are formed in N-terminus and the rest part of the protein remains unfolded. (C) αSyn binds to cellular membrane with its membrane binding site in N-terminus. It is found bound to membranes by two α-helices.

amyloid fibrils in fibrillation condition in vitro [31]. To verify the fibrillation kinetics of each αSyn monomer, Thioflavin T (ThT) binding assay was performed every day for 19 days. WT αSyn fibrillation kinetics showed increased ThT fluorescence and the peak ThT fluorescence reached its peak at day 5. In contrast, V40G mutant αSyn showed very low ThT value during the fibrillation experiment. There was no rising curve in ThT fluorescence until the end of the kinetics observation, meaning V40G does not form the β-sheet enriched fibril (Figure 3A). CD spectroscopy showed that only 'aged' WT exhibited β-sheet conformation-enriched structure with minimum absorbance at 218 nm. 'Aged' V40G exhibited CD spectra characteristic for random coil similar to the 'fresh' WT and V40G proteins with minimum absorbance at about 200 nm (Figure 3B). The Aged-WT and V40G proteins were added as seeds in fibrillation assay, and their ThT binding kinetics were monitored for 7 days (Figure 3C). With aged-WT as seeds, the lag phase reduced drastically and reached maximal ThT fluorescence earlier than the 'no seeds' condition. On the other hand, using aged-V40G as seeds showed no increase in ThT fluorescence which means that aged-V40G prevented αSyn fibrillation. These results demonstrate that aged-V40G is not capable of seeding, or even blocking, the aggregation of αSyn.

The purpose of the study

The current mainstream thoughts on the aggregate transmission involve the template seeding as the mechanism of aggregate amplification in the recipient

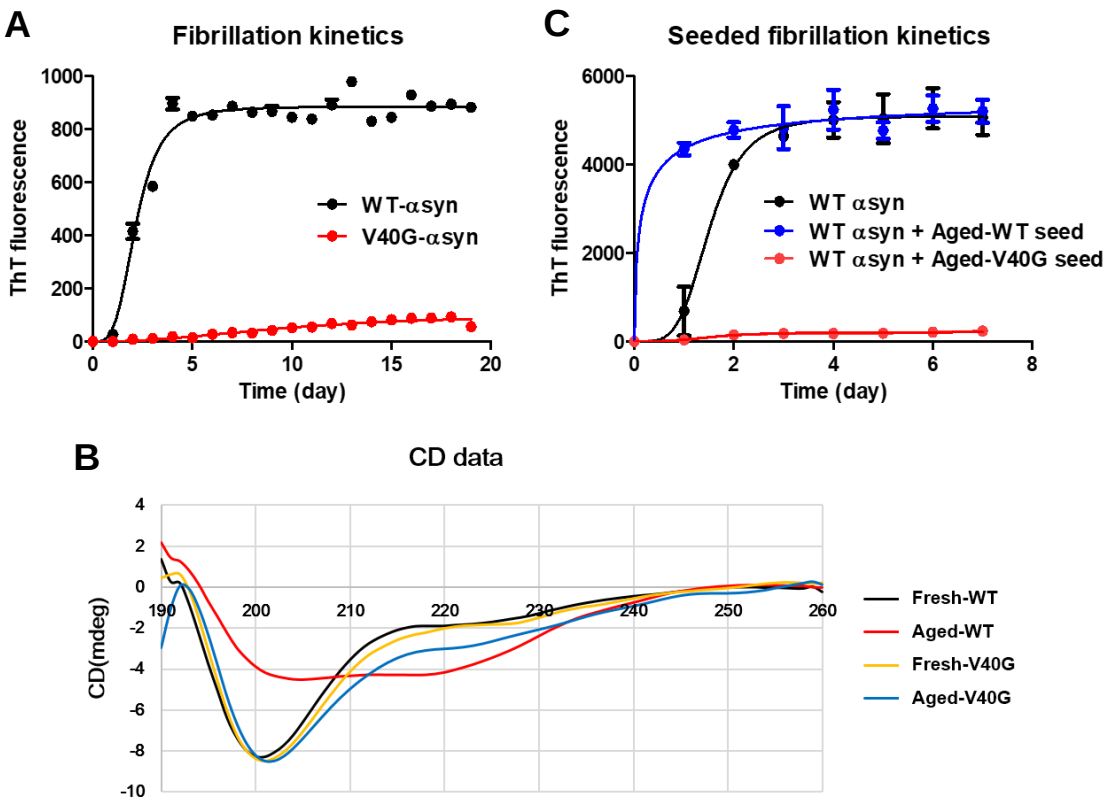

Figure 3. Characteristics of WT and V40G αSyn

(A) Fibrillation kinetics of WT and V40G αSyn. (B) CD spectroscopy data which shows each structure of fresh, aged WT and V40G αSyn. (C) Seeded fibrillation results of each condition.

neurons. However, the template seeding hypothesis has not been completely proven to date. The purpose of my study is to verify whether the template seeding mainly work as the mechanism of aggregate amplification. The seeding blocking property of the V40G variant allows me to do authenticity test about template seeding hypothesis. To this end, I performed seeding assay, measuring αSyn aggregate transmission level with detected fluorescence signal using the dual-cell Bimolecular Fluorescence Complementation (BiFC) system.

MATERIALS & METHODS

1. Materials

The following antibodies were used in this study: p62 monoclonal antibody (1:1,000 dilution; BD Transduction Laboratories, #c2384-0B; Swampscott, MA), ubiquitin polyclonal antibodies (1:1,000 dilution; Dako; Glostrup, Denmark and Chemicon; Temecula, CA), cathepsin D (CTSD) monoclonal antibody (1:1000 dilution; Abcam, ab6313), Gcase (GBA) monoclonal antibody (1:1000 dilution; Abcam, ab128879), Arylsulfatase A (ARSA) monoclonal antibody (1:1000 dilution; Abcam, ab 174844), Lysosome-associated membrane protein 2 (LAMP2) monoclonal antibody (1:1000 dilution; Abcam, ab25631), Protein disulfide-isomerase (PDI) monoclonal antibody (1:1000 dilution; BD Transduction Laboratories, #610946), Heat shock protein 70 (Hsp70) monoclonal antibody (1:5000 dilution; Stressgen, #ADI-SPA-822), Secretogranin II (SGII) polyclonal antibody (1:100 dilution; Santa Cruz Biotechnology, sc-1490), and β-actin monoclonal antibody (1:10,000 dilution; Sigma). Horse radish peroxidase (HRP)-conjugated goat anti-mouse immunoglobulin G (IgG; H+L) (1:3000 dilution; Bio-Rad Laboratories, 172–1011, Hercules, CA, USA) and HRP-conjugated goat anti-rabbit IgG (H+L) (1:3000 dilution; Bio-Rad Laboratories). Fluorescence dye-conjugated goat anti-rabbit IgG and anti-mouse IgG were purchased from Jackson Immunoresearch Laboratories (1:500 dilution; West Grove, PA). Thioflavin T (ThT) and protease inhibitor cocktail were purchased from Sigma-Aldrich (St Louis, MO, USA). Fluorescein-conjugated dextran (10 000 molecular weight; D-1821), TO-PRO-3 iodide (T3605) and

LysoTracker Red DND-99 (L-7528) were purchased from Invitrogen (Carlsbad, CA, USA).

2. Cell culture and Stable cell line

SH-SY5Y human neuroblastoma cell lines were as described previously [32]. Briefly, cells were subcultured at 37°C in humidified air with 5% CO2 in Dulbecco's modified Eagle medium (DMEM) containing 10% fetal bovine serum, 100 units ml−1 penicillin and 100 units ml−1 streptomycin every 2 days. To generate stable cell lines, SH-SY5Y human neuroblastoma cells (ATCC CRL-2266; Manassas, VA) were transfected with Venus1-αSyn (V1S) or αSyn-Venus2 (SV2) plasmid (kind gifts from Dr Pamela McLean, Massachusetts General Hospital, Charlestown, MA) using electroporation. Transfected cells were selected with 600 μg ml−1 G418 (Invitrogen) for 2–3 weeks until colonies emerged. The stable cell lines were maintained with 200 μg ml−1 G418. For co-culture, V1S and SV2 stable cells (60,000 cells each) were mixed in a coverslip and cultured for 3 days. To determine the continuous transmission of αSyn, the mixture of V1S and SV2 cells was subcultured every 2 days (48 h).

3. Purification of recombinant wild type and V40G mutant αSyn and Fibril preparation

Two types of human αSyn, WT and V40G, were expressed from the pDualGC vector and induced with 0.1 mM IPTG for 3 hours at 37°C when the absorbance of the E. coli strain BL21 (DE3) (RBC Korea, Seoul, Korea) culture reached 0.6 at 600 nm. The

cells were pelleted and resuspended in 20 mM sodium phosphate buffer (pH 7.4) for sonication and were subsequently boiled at 100°C for 20 min, then centrifuged at 10,000 × g for 10 min. The supernatant was subjected to anion-exchange chromatography and Superdex-200 gel filtration column chromatography for further purification. The purified αSyn was dialyzed against distilled water and subsequently lyophilized.

For monomer preparation (referred as “Fresh”), lyophilized αSyn was reconstituted in phosphate-buffered saline (PBS; #CAP08-050, GenDEPOT, Katy, TX, USA), then subjected to ultrafiltration using a 100,000 molecular weight cut-off centrifugal device (Pall, New York, USA). For fibrillation (referred as “Aged”), WT or V40G αSyn (200 μM in PBS) was incubated at 37°C for 19 days with constant shaking at 1,050 rpm in a Thermomixer C (#5382000015, Eppendorf, Hamburg, Germany). When used as seeds, the fibrils were sonicated for 1 min (Amplitude 30%) before treated to cells.

4. Thioflavin T binding assay

Forty microliters of a 10 μM recombinant αSyn sample or fibrillation products was added to 50 μl of 10 μM ThT solution in glycine-NaOH (pH 8.5). After 5 min of incubation, fluorescence was measured at 450 nm excitation and 490 nm emission settings.

5. Circular dichroism spectroscopy

The samples were diluted in PBS at 15 μM and analyzed using a Chirascan plus spectropolarimeter (Applied Photophysics, Randalls Rd, Leatherhead, UK).

6. Seeding assay in Venus cell-lines

For seeding effect of exogenous sonicated aged-WT or V40G mutant αSyn, the co-cultured V1S and SV2 cells were treated with 0.1 μM aged-WT/V40G for 3 days.

7. Immunofluorescent Cell staining

Cells grown on poly-L-Lysine-coated coverslips were fixed in 4% paraformaldehyde in PBS and permeabilized in 0.1% Triton X-100 in PBS. After incubation in blocking solution (5% bovine serum albumin/3% goat serum in PBS), primary antibodies diluted in blocking solution were added to the cells. After washing, cells were incubated with fluorescent dye-conjugated secondary antibodies. Nuclei were stained with TOPRO-3 iodide (Invitrogen). Cells were mounted onto slide glasses in the presence of Prolong Gold Antifade Reagent (Invitrogen). Zeiss 63X (N.A. 1.4) objective on an Axiovert 35 microscope (Zeiss) with an attached MRC1024 laser scanning confocal microscope (LSCM) system (BioRad) was used for observation of cells.

8. Galectin-3 transfection using electroporation

Each V1S and SV2 cell line were transfected with galectin-3 expressing plasmid DNA through the electroporation method with 4D-Nucleofector™ System (LONZA,

Switzerland). Every step of the electroporation was performed as offered protocol from LONZA using SF Cell Line 4D-Nucleofector® X Kit L (LONZA, Switzerland).

9. Characterization of lysosomal dysfunction

To determine the degradation ratio of internalized dextran, cells were incubated with 20 μg ml−1 of fluorescein isothiocyanate-labelled dextran (Invitrogen) for 2 h. After washing with DMEM, cells were incubated with fresh growth media for 30 min and 1 hour, then fixed with a 4% paraformaldehyde (PFA) solution. For imaging of the lysotracker-positive compartment, cells were stained with 75 nM lysotracker solution in dimethyl sulphoxide (Lysotracker Red DND-99; Invitrogen) diluted in growth media, and incubated for 1 h at 37°C in a CO2 incubator. After washing with ice-cold PBS, cells were fixed in a 4% PFA solution. The fluorescence intensity was measured using Zeiss 63X (N.A. 1.4) objective on an Axiovert 35 microscope (Zeiss) with an attached MRC1024 laser scanning confocal microscope (LSCM) system (BioRad).

10. Preparation of cell extracts and lysosome fraction

After washing with ice-cold PBS, cells were lysed in extraction buffer (1% Triton X-100, 1% (v/v) protease inhibitor cocktail in PBS). Cell lysates were incubated on ice for 10 min and centrifuged at 16,000 x g for 10 min. The Triton X-100 insoluble fraction was resuspended in 1X Laemmli sample buffer and sonicated briefly. For preparation of lysosome fraction, cells were washed with ice-cold Hank's Balanced Salt Solution (HBSS) buffer (Gibco™) and harvested with extraction buffer (1% (v/v)

protease inhibitor cocktail in HB buffer; 250mM sucrose, 10mM KCl, 1mM EDTA, 10mM HEPES, pH 7.4). Harvested cells were homogenated with Dounce glass homogenizer and incubated on ice for 10 min. Centrifuged at 1,000 x g for 10 min to pellet nuclei and remaining intact cells. The post-nuclear supernatant was ultracentrifuged at 100,000 x g for 2 hour with Table-top Ultracentrifuge Optima TLX (Beckman Coulter, Inc., USA). Pellets were washed with the extraction buffer, then resuspended in 1X Laemmli sample buffer and sonicated briefly.

11. Immunoblotting

Immunoblotting was performed as previously described [33]. Protein samples were loaded onto 12% SDS-PAGE gels. Image detection was performed using an Amersham imager 600 (GE Healthcare Life Sciences, Marlborough, MA, USA), and Multi Gauge (v3.0) software (Fujifilm, Tokyo, Japan).

12. Quant RNA-seq analysis

12-1. RNA isolation

Total RNA was isolated using Trizol reagent (Invitrogen). RNA quality was assessed by Agilent 2100 bioanalyzer using the RNA 6000 Nano Chip (Agilent Technologies, Amstelveen, The Netherlands), and RNA quantification was performed using ND-2000 Spectrophotometer (Thermo Inc., DE, USA).

12-2. Library preparation and sequencing

For control and test RNAs, the construction of library was performed using SENSE 3' mRNA-Seq Library Prep Kit (Lexogen, Inc., Austria) according to the manufacturer's instructions. In brief, each 500 ng total RNA were prepared and an oligo-dT primer containing an Illumina-compatible sequence at its 5' end was hybridized to the RNA and reverse transcription was performed. After degradation of the RNA template, second strand synthesis was initiated by a random primer containing an Illumina-compatible linker sequence at its 5' end. The double-stranded library was purified by using magnetic beads to remove all reaction components. The library was amplified to add the complete adapter sequences required for cluster generation. The finished library is purified from PCR components. High-throughput sequencing was performed as single-end 75 sequencing using NextSeq 500 (Illumina, Inc., USA).

12-3. Data analysis

SENSE 3' mRNA-Seq reads were aligned using Bowtie2 version 2.1.0 [34]. Bowtie2 indices were either generated from genome assembly sequence or the representative transcript sequences for aligning to the genome and transcriptome. The alignment file was used for assembling transcripts, estimating their abundances and detecting differential expression of genes. Differentially expressed gene were determined based on counts from unique and multiple alignments using EdgeR within R version 3.2.2 (R development Core Team, 2011) using BIOCONDUCTOR version 3.0 [35]. The RT (Read Count) data were processed based on Global normalization method using the Genowiz ™ version 4.0.5.6 (Ocimum Biosolutions, India). Gene classification was based on searches done by DAVID (http://david.abcc.ncifcrf.gov/) and Medline

databases (http://www.ncbi.nlm.nih.gov/).

13. Network analysis

13-1. Gene ontology

Searching work with selected DEGs from the Quant RNA-seq data was done by DAVID (http://david.abcc.ncifcrf.gov/).

13-2. KEGG pathway

KEGG pathway searching work with selected DEGs was performed as published protocol [36]. KEGG is made available at both the KEGG main website (http://www.kegg.jp/) and the GenomeNet mirror website (http://www.genome.jp/kegg/).

13-3. Cytoscape

Analysis work with Cytoscape in this paper was performed as published protocol [37]. For simplest operation, Cytoscape can be executed over the web via Java Web Start by navigating to http://www.cytoscape.org/nature.protocols/ and clicking on the web start link. See http://java.sun.com/products/javawebstart/ for more information on running Java Web Start applications. Alternatively, Cytoscape can be installed on a local computer.

14. Quantification and Statistical analysis

Values shown in the figures are presented as mean±s.e.m. To determine the statistical significance, P values were calculated by one-way ANOVA with Tukey's multiple comparison test using GraphPad Prism version 5.02 software.

RESULTS

The template seeding may not be the crucial mechanism of the intercellular aggregate propagation

In this study, I define fresh-WT and fresh-V40G αSyn as newly prepared monomeric proteins, while aged-WT and aged-V40G as the proteins incubated at 37℃ for 9 days with constant agitation [30]. To verify whether the αSyn aggregate propagation depends on the template seeding, aggregate propagation assay was performed in the dual-cell BiFC system. About this system, it was previously described [38] and explained briefly in Figure 4A. Cells were incubated with fresh-WT, V40G and aged-WT, V40G respectively. Venus fluorescence in this system indicates the extent of transmission between cells. Results showed that the fluorescence signal was increased in both aged-WT and aged-V40G treatment condition even though the aged-V40G has no seeding activity (Figure 4B). Data values were represented as the percentage of Venus-positive cells (Figure 4C). This indicates that template seeding may not be a crucial mechanism in the propagation of αSyn aggregates.

Aged αSyn did not affect the selective autophagy, nor the ER-Golgi biosynthetic pathway

Next, several approaches were performed to elucidate the actual mechanism by which the transferred aSyn aggregates induce the aggregation in the recipient

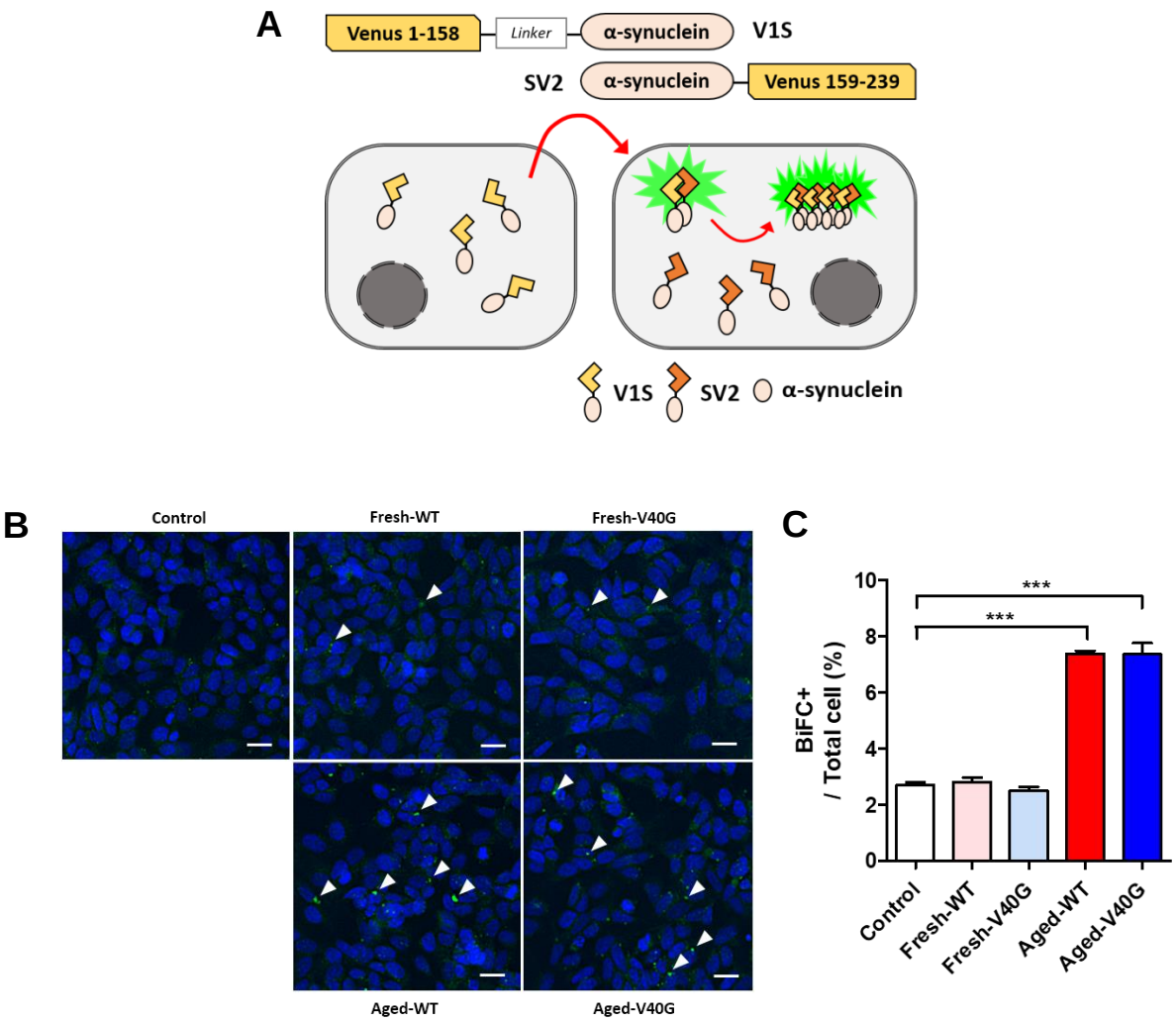

Figure 4. Seeding assay result of fresh and aged-WT/V40G in Venus cell-lines

(A) Schematic representation of BiFC system using cells stably overexpressing V1S (Venus 1-158-αSyn) or SV2 (αSyn-Venus 159-239). Under co-culture condition, neuron to neuron transfer and aggregation of αSyn can be observed by the reconstitution of green fluorescence. (B) Cell-to-cell transmission of αSyn in the dual-cell BiFC system. Cells were incubated with 0.1μM of fresh-WT, fresh-V40G, aged-WT, aged-V40G or PBS for 3 days. BiFC positive aggregates are indicated by arrowheads. Scale bars, 20 μm. (C) Quantification of BiFC-positive cells shown in (B).

cells. Some intracellular mechanisms were selected as candidates for the mechanism of aggregation in the recipient cells. Increased transmission of αSyn aggregates might be a consequence of aggravation of protein degradation via proteasome and lysosomal-autophagy.

First, selective autophagy is one of the major intracellular degradation mechanisms of cellular trashes like misfolded proteins or damaged mitochondria. Those are recognized by ubiquitin proteins and recruited into the autophagosome by p62 protein. This degradation function of selective autophagy is crucial for maintaining the normal cellular protein metabolism. To verify whether the function of selective autophagy is impaired after each fresh or aged αSyn treatment, immunoblot analysis of ubiquitin and p62 protein levels in cell lysates was performed. Immunoblot band intensities were quantified, normalized with β-actin (Figure 5B). The result showed that there were no differences of ubiquitin and p62 protein levels in both Triton-X soluble and insoluble fractions (Figure 5A).

Next, I examined endoplasmic reticulum-Golgi apparatus (ER-Golgi) biosynthetic pathway. Secretogranin-II (SGII) is a neuroendocrine secretory granule protein, which is the precursor for biologically active peptides [39]. It is located in large dense core vesicles of endocrine, neuroendocrine and neuronal tissues [39]. Immunoblot analysis was conducted to verify the quantity of secreted proteins in the culture media. SGII was detected as secreted protein marker. Culture media were collected after the fresh or aged αSyn treatment. The levels of SGII showed no differences which suggested the fresh or aged αSyn did not affect the biosynthetic pathway (Figure 5C and D).

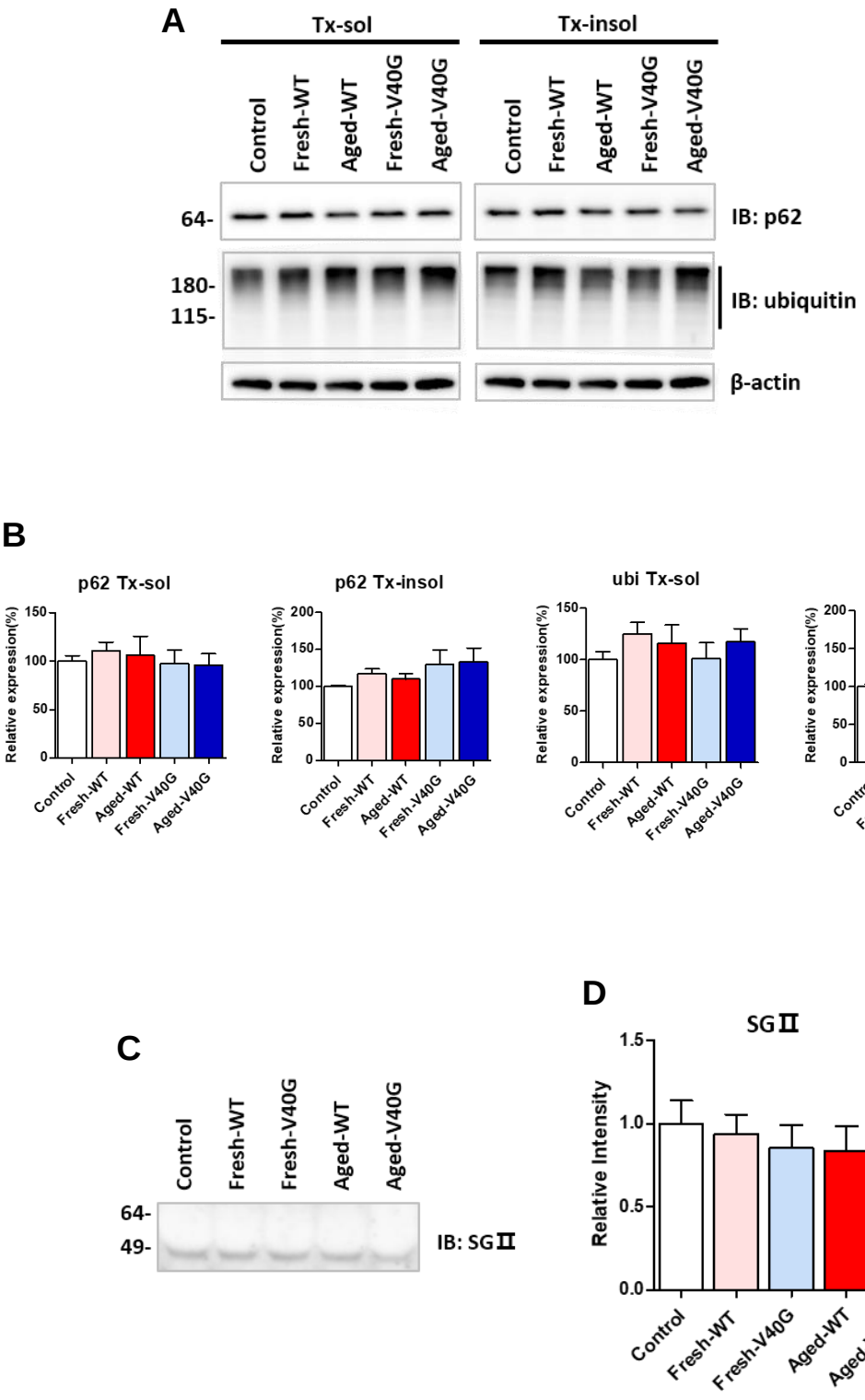
A
Tx-sol
Tx-insol
Control
Fresh-WT
Aged-WT
Fresh-V40G
Aged-V40G
64-
180-
115-
IB: p62
IB: ubiquitin
β-actin
B
p62 Tx-sol
p62 Tx-insol
ubi Tx-sol
ubi Tx-insol
Relative expression(%)
C
IB: SGⅡ
D
SGⅡ
Relative Intensity

Figure 5. Immunoblot analysis of selective autophagy and ER-Golgi biosynthetic pathway

(A) Immunoblot analysis of p62, ubiquitin in cell lysates shows no differences in each treat condition. (B) Quantification of immunoblot images in (A). Those band intensities were normalized with β-actin. (C) SGII levels which indicates ER-Golgi biosynthetic pathway degree also showed no differences in each treat condition. (D) Quantification of immunoblot images in (C).

Treatment with the aged αSyn reduced the rate of the endo-lysosomal degradation

Next, the endo-lysosomal pathway was tested whether it was affected by the extracellular αSyn. Cells were incubated with fluorescein isothiocyanate-labelled dextran after the fresh or aged αSyn treatment. Degradation rates of internalized dextran were measured at different time points, which represented the endo-lysosomal degradation rate. Fresh-WT and fresh-V40G αSyn treated cells showed the same result with the control dextran degradation rate. But both aged-WT and aged-V40G αSyn treated cells showed reduced degradation rates of the internalized dextran. After the 1 hour degradation time, there were still green signals remained in aged αSyn treated cells (Figure 6A). In quantification graph, the difference of dextran degradation rate caused by aged αSyn was shown more clearly (Figure 6B). This indicates that the aged αSyn makes some alteration in the endo-lysosomal pathway, reducing endo-lysosomal degradation rate.

Lysosomal integrity was intact after the incubation with the aged αSyn

Based on the dextran degradation result, there are some considerable reasons that are affected by aged αSyn and make the endo-lysosomal degradation rate reduce. One is the lysosome state. If there is lysosomal rupture, lysosomal membrane permeabilization (LMP), by treated with aged αSyn, acidic condition of the lysosome cannot be maintained. Then lysosomal enzymes cannot work normally and show

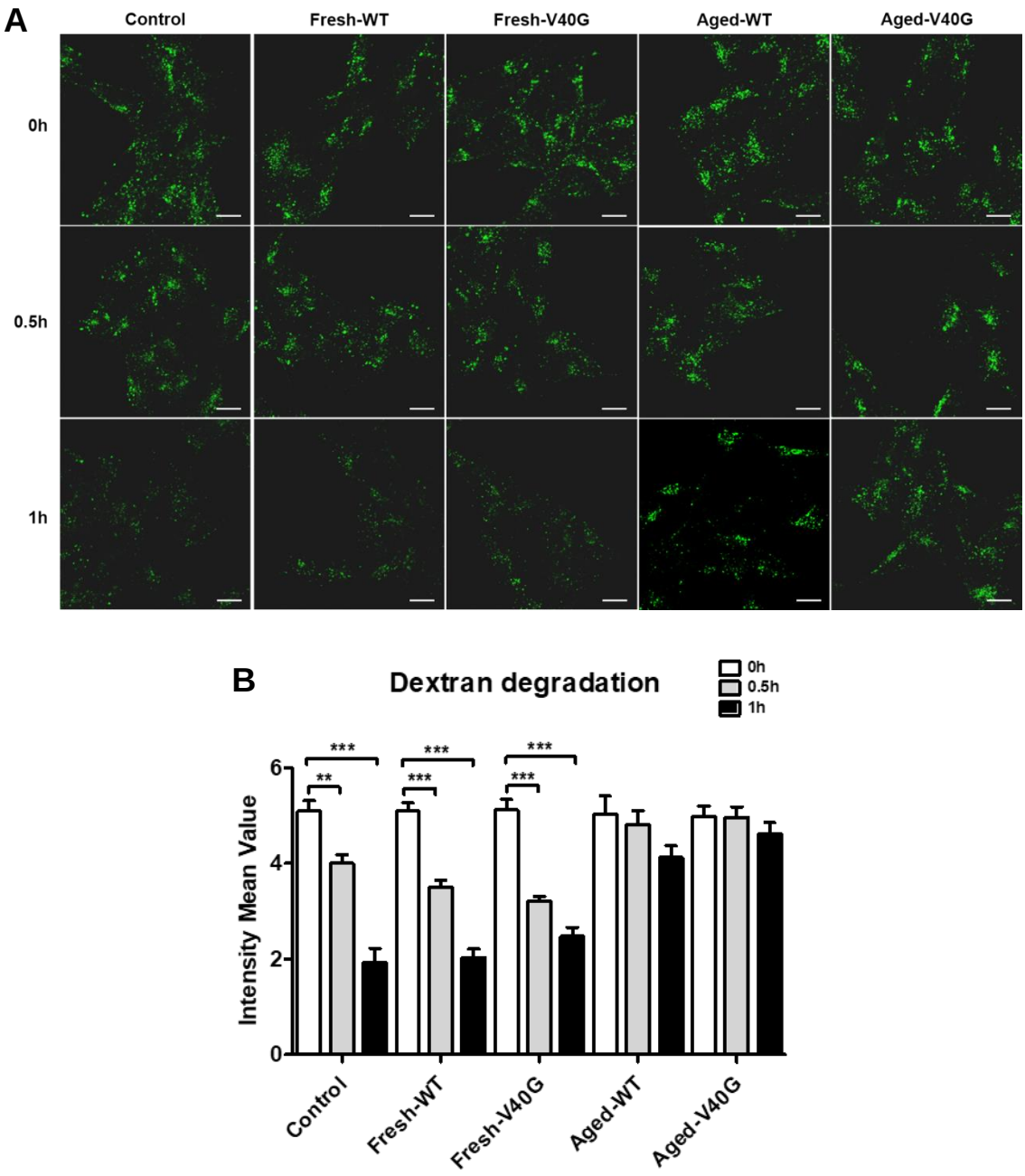

Figure 6. Endo-lysosomal degradation rates in each αSyn treat condition

(A) Alteration in the degradation rate of internalized fluorescein-conjugated dextran. Scale bar: 20 μm. (B) Both aged-WT and aged-V40G αSyn treated cells show lower dextran degradation rate than others. **p<0.01, ***p<0.001

reduced degradation function for that reason. To identify the lysosome state, lysosome rupture assay was conducted by immunoblot analysis and galectin-3 puncta assay. For the immunoblot analysis, several lysosomal hydrolases (Gcase: GBA, cathepsin D; CTSD, and arylsulfatase A; ARSA) were chosen and other markers (lysosome-associated membrane protein 2; LAMP2, protein disulfide isomerase; PDI, and heat shock protein 70; Hsp70) were also chosen. Cell lysates were separated into the cytosol and vesicles by ultracentrifugation. The vesicle fractions contain lysosomes. In the immunoblot analysis, lysosomal hydrolase were detected in the vesicles, not in the cytosol (Figure 7A). Normalized with β-actin, there were no significant differences between fresh or aged αSyn treated conditions (Figure 7B). This indicates that lysosome is intact after the incubation with aged αSyn. To verify this result via cell imaging, the galectin-3 puncta assay was performed. V1S and SV2 cells were transfected to express mCherry-conjugated galectin-3. Galectin-3 is the lectin family protein that contains a carbohydrate-recognition-binding domain (CRD), enabling the specific binding of β-galactosides [40, 41]. Galectin-3 localizes cytoplasm and β-galactoside localizes the inner membrane of lysosome. When LMP is induced, galectin-3 recognizes β-galactosides and this is observed as red puncta in cells through the confocal images [42]. Results of galectin-3 puncta assay showed diffused red signal in cytosol and it was hard to find red puncta in cells (Figure 7C). This correlated with the immunoblot analysis result. With all, lysosome state was not affected by the aged αSyn and this is not the reason of the reduced endo-lysosomal degradation rate.

Lysosome acidification was intact

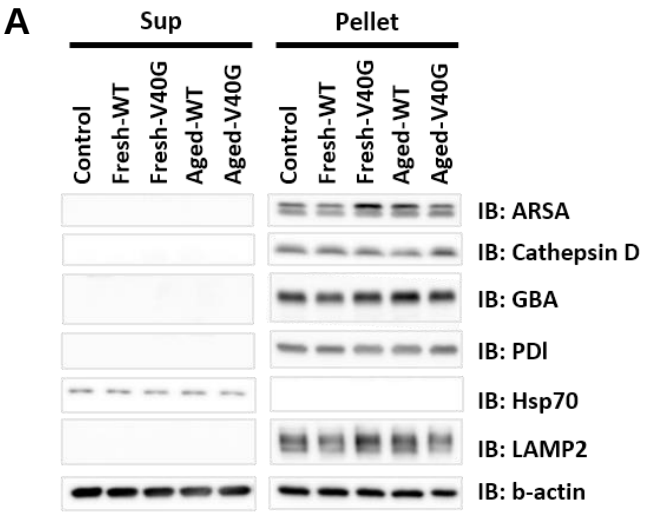
A
Sup
Pellet
Control
Fresh-WT
Fresh-V40G
Aged-WT
Aged-V40G
IB: ARSA
IB: Cathepsin D
IB: GBA
IB: PDI
IB: Hsp70
IB: LAMP2
IB: b-actin

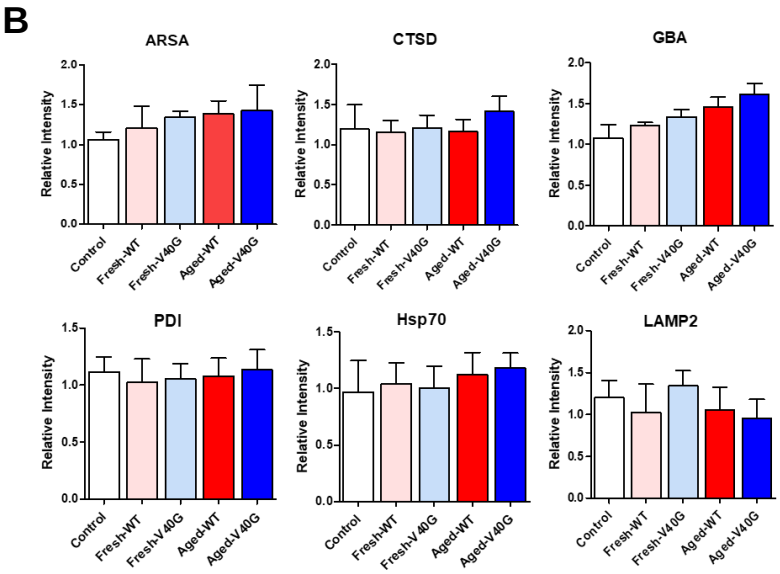
B
ARSA
CTSD
GBA
PDI
Hsp70
LAMP2
Relative Intensity
Control
Fresh-WT
Fresh-V40G
Aged-WT
Aged-V40G

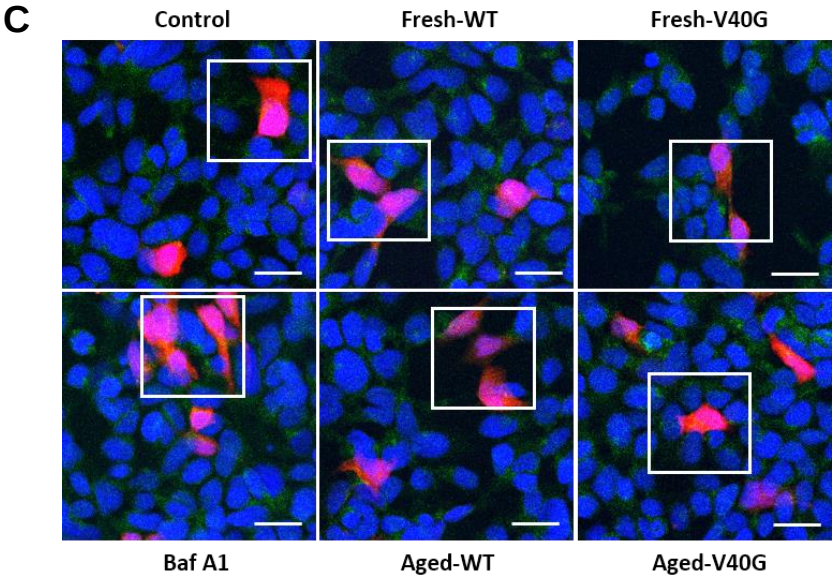
C
Control
Fresh-WT
Fresh-V40G
Baf A1
Aged-WT
Aged-V40G

Figure 7. Lysosome rupture assay results in immunoblot and galectin-3 puncta analysis

(A) Immunoblot analysis of several lysosomal hydrolases. PDI is a biological marker for endosome, and Hsp70 is for the confirmation of sup contamination in prepped lysosome sample. Those band intensities were normalized with beta-actin and showed in (B). (B) Quantification of the immunoblot images. (C) Galectin-3 puncta analysis shows no differences between control and fresh or aged αSyn treated samples. Scale bar: 20 μm.

Lysosomal acidification can be another option of causative factor for the alteration of the endo-lysosomal degradation. Even fluid cargoes finally reach the lysosome through the endo-lysosomal pathway; it could not be degraded when the acidification of lysosome is not at normal state. Lysosomal activity depends on the maintaining of the acidic condition of lysosome because enzymes in lysosome show their activity in acidic condition [43, 44]. Lysotracker-Red staining was conducted to measure lysosomal acidification after each fresh or aged αSyn treatment. Confocal images of the lysosome acidification assay showed that there was no difference in percentages of the red puncta containing cells between control and fresh or aged αSyn treated cells (Figure 8A). Bafilomycin A1, vacuolar H+ ATPase; V-ATPase inhibitor that inhibits acidification and protein degradation in lysosomes [45], was used for negative control. Values of the red puncta containing cells in each condition were quantified (Figure 8B). This suggests that lysosome acidification was not affected by the aged αSyn and this is also not the reason of the reduced endo-lysosomal degradation rate.

Reduction in the endo-lysosomal degradation was a long-term effect of the aged αSyn

To examine the nature of the defects in the endo-lysosomal pathway, dextran degradation assay was performed again with different αSyn incubation times. This was for verifying whether the alteration in the endo-lysosomal degradation was by short-term effect or long-term effect of the aged αSyn. After 1 hour, 1 day, and 3

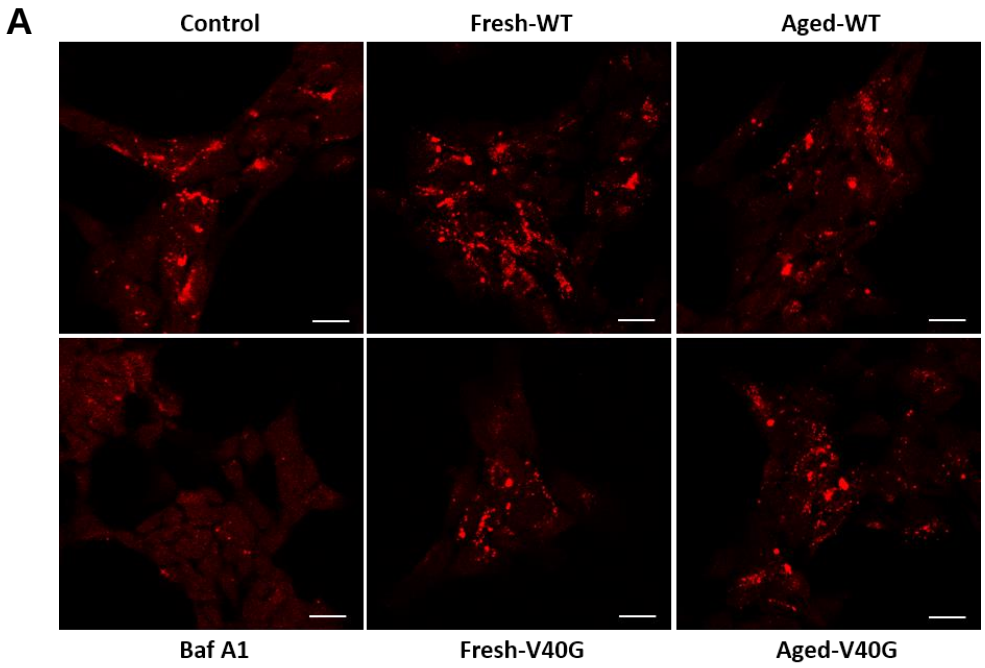

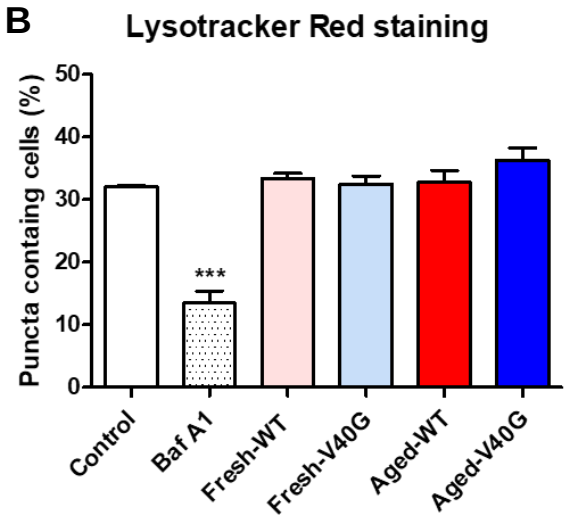

Figure 8. Lysosome acidification assay in each αSyn treat condition

(A) LysoTracker Red DND-99 staining result shows no differences. Bafilomycin A1 was used for the negative control. Scale bar: 20 μm. (B) Quantification of the red puncta containing cells in total cells. ***p<0.001

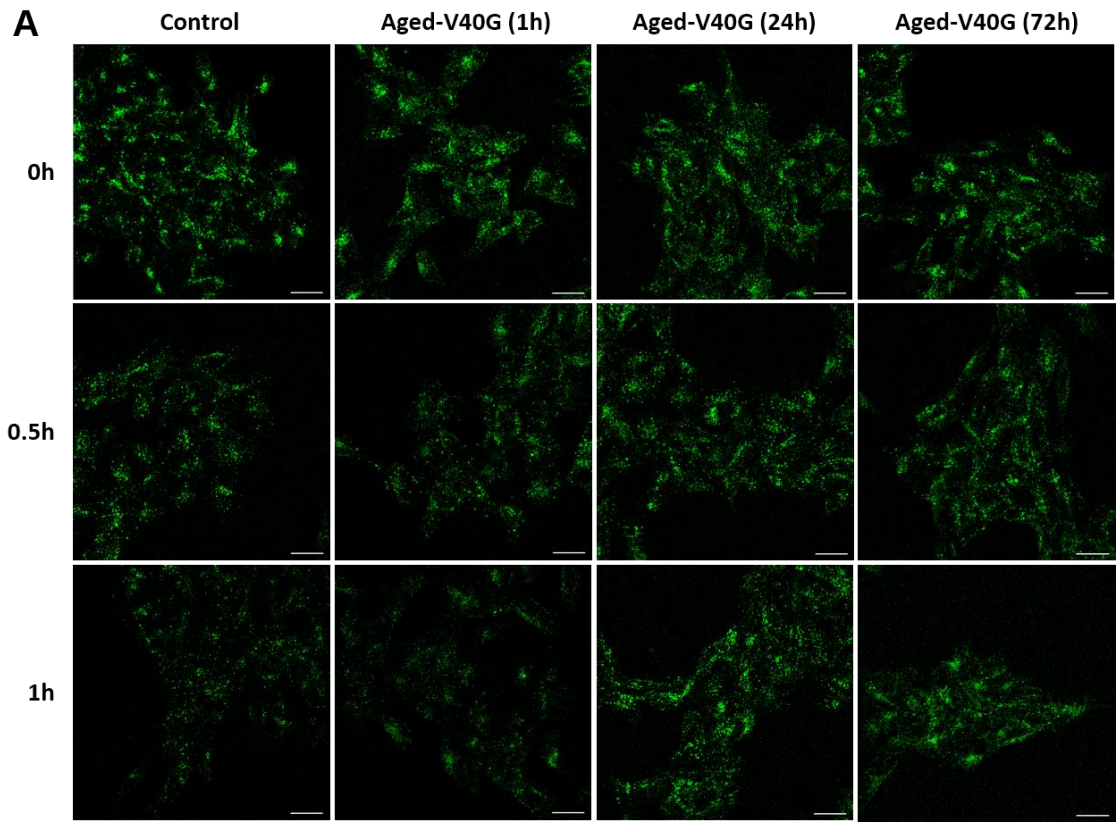
A
Control
Aged-V40G (1h)
Aged-V40G (24h)
Aged-V40G (72h)
0h
0.5h
1h

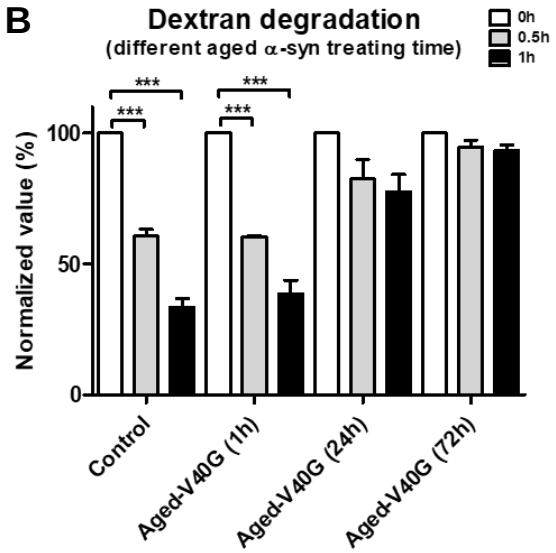
B
Dextran degradation
(different aged α-syn treating time)
0h
0.5h
1h
***
***
***
***
Normalized value (%)
100
50
0
Control
Aged-V40G (1h)
Aged-V40G (24h)
Aged-V40G (72h)

Figure 9. Dextran degradation result after treatments of the aged αSyn for different incubate times

(A) Images of internalized dextran degradation in each cell culture which aged αSyn treated time differently. (B) Quantification of dextran degradation rates of (A). ***p<0.001

days of aged αSyn incubation, the result showed that the degradation rate was similar until the 1 day incubation (Figure 9). But the degradation rate reduced in the result of 3 days incubation. From this, the alteration in endo-lysosomal pathway was the result of long-term effect caused by aged αSyn.

Transcriptome analysis of the cells exposed to the aged aSyn

To gain insights into the mechanism of extracellular αSyn-induced aggregation in the recipient cells, quant-mRNA sequencing (RNA-seq) was conducted. Samples for the RNA-seq were prepared, control and aged-V40G αSyn treated cells in triplicate. List of differentially expressed genes (DEG) was shown in Table 1. Fold changes are expressed as the value of $\log_2$. RNA-seq data allowed us to quantitatively compare transcriptomic changes in aged-V40G αSyn treated cells with control. Sequencing data was analyzed by DAVID for gene ontology and KEGG pathway (Table 2 and 3) and Cytoscape (for transcription factor and its target genes interaction).

Through the KEGG pathway results, a transcription factor MYC seemed having some potential as a starting point in the alteration of endo-lysosomal pathway. So, a map showing interactions transcription factors and their target genes was drawn by Cytoscape (Figure 10A). As expected, the map showed that MYC was located as a crucial transcription factor in the RNA-seq data. Other transcription factors including FOSB were also shown together in the map. Genes which were regulated by MYC and FOSB were shown as a list (Table 4). Based on this map, genes were categorized

UP regulated 224 genes				DOWN regulated 223 genes			
Entrez ID	Gene symbol	Fold change	p value	Entrez ID	Gene symbol	Fold change	p value
2	A2M	0.42286	0.00225	95	ACY1	-0.47160	0.00538
361	AQP4	0.66470	0.00298	314	AOC2	-0.36683	0.02112
549	AUH	0.39205	0.00429	412	STS	-0.57254	0.00537
558	AXL	0.57391	0.00570	622	BDH1	-0.37801	0.00162
634	CEACAM1	0.83331	0.00191	666	BOK	-0.57185	0.00116
716	C1S	0.73869	0.00340	741	ZNHIT2	-0.40218	0.00239
730	C7	0.41111	0.00869	797	CALCB	-0.39237	0.01220
945	CD33	0.42697	0.01128	1307	COL16A1	-0.36886	0.00235
1360	CPB1	0.46350	0.01209	1357	CPA1	-0.68584	0.00292
1427	CRYGS	0.47917	0.00199	1392	CRH	-0.61612	0.00102
1815	DRD4	0.58318	0.00240	1633	DCK	-0.49656	0.00710
1901	S1PR1	0.42697	0.00219	1907	EDN2	-0.41590	0.01291
2185	PTK2B	0.40189	0.01515	1959	EGR2	-0.39033	0.00807
2256	FGF11	0.49353	0.00602	2012	EMP1	-0.49026	0.00781
2354	FOSB	0.60481	0.00256	2048	EPHB2	-0.49941	0.01101
2537	IFI6	0.38912	0.01838	2052	EPHX1	-0.48938	0.00842
2803	GOLGA4	0.57059	0.00017	2184	FAH	-0.44735	0.01147
2886	GRB7	0.63207	0.00091	2870	GRK6	-0.41391	0.01187
2979	GUCA1B	0.47946	0.00036	3078	CFHR1	-0.59506	0.00592
3074	HEXB	0.36161	0.01220	3222	HOXC5	-0.53133	0.00584
3162	HMOX1	0.44734	0.00165	3400	ID4	-0.41590	0.01412
3600	IL15	0.56121	0.00232	3664	IRF6	-0.74654	0.00179
3750	KCND1	0.46932	0.00317	4171	MCM2	-0.42434	0.00444
3770	KCNJ14	0.52990	0.00351	4174	MCM5	-0.47494	0.01177
3821	KLRC1	0.42316	0.01244	4234	METTL1	-0.47568	0.00624
3995	FADS3	0.48566	0.01083	4609	MYC	-0.53918	0.00314
4069	LYZ	0.53857	0.00869	4702	NDUFA8	-0.40009	0.00429
4072	EPCAM	0.46350	0.00671	4920	ROR2	-0.39799	0.00186
4647	MYO7A	0.63274	0.00503	5001	ORC5	-0.70954	0.00153
4820	NKTR	0.45694	0.00338	5211	PFKL	-0.40055	0.01072
5016	OVGP1	0.46329	0.00265	5313	PKLR	-0.40385	0.00075
5141	PDE4A	0.45780	0.00645	5368	PNOC	-0.49859	0.00522
5261	PHKG2	0.49859	0.00633	5576	PRKAR2A	-0.46004	0.00423
5342	PLGLB2	0.50781	0.00118	5799	PTPRN2	-0.42200	0.00635
5354	PLP1	0.53857	0.00888	6041	RNASEL	-0.36683	0.00596
5367	PMCH	0.38076	0.00968	6236	RRAD	-0.57185	0.00430
5565	PRKAB2	0.39350	0.01376	6293	VPS52	-0.40300	0.01553
5873	RAB27A	0.50429	0.00378	7027	TFDP1	-0.47334	0.00118
5926	ARID4A	0.48061	0.00341	7066	THPO	-0.73552	0.00168
6016	RIT1	0.38415	0.01058	7083	TK1	-0.62257	0.00031
6334	SCN8A	0.37607	0.00925	7374	UNG	-0.49065	0.00654
6335	SCN9A	0.41082	0.01584	7390	UROS	-0.40143	0.00708
6414	SEPP1	0.38014	0.01644	7442	TRPV1	-0.43876	0.00630
6450	SH3BGR	0.55089	0.00172	7554	ZNF8	-0.46908	0.00813
6671	SP4	0.35680	0.01891	8045	RASSF7	-0.37861	0.01906
7008	TEF	0.44252	0.01177	8074	FGF23	-0.58143	0.00080
7060	THBS4	0.74871	0.00186	8295	TRRAP	-0.40613	0.01655
7123	CLEC3B	0.49877	0.00366	8347	HIST1H2BC	-0.37580	0.00406
7567	ZNF19	0.39414	0.00701	8362	HIST1H4K	-0.68308	0.00440
7582	ZNF33B	0.41773	0.00750	8363	HIST1H4J	-1.06827	0.00117
7675	ZNF121	0.75014	0.00099	8636	SSNA1	-0.44280	0.01002
7768	ZNF225	0.59846	0.00226	8819	SAP30	-0.50731	0.00348
7769	ZNF226	0.41289	0.01582	8851	CDK5R1	-0.39892	0.00356
7782	SLC30A4	0.35614	0.00520	8994	LIMD1	-0.44428	0.01121
8497	PPFIA4	0.47665	0.00361	9024	BRSK2	-0.44092	0.00665
8608	RDH16	0.75589	0.00160	9047	SH2D2A	-0.49026	0.00061
8630	HSD17B6	0.35427	0.00699	9048	ARTN	-0.36886	0.01632
8690	JRKL	0.48781	0.00012	9136	RRP9	-0.41984	0.00536
8748	ADAM20	0.36937	0.00514	9310	ZNF235	-0.50573	0.00421
9068	ANGPTL1	0.61151	0.00165	9468	PCYT1B	-0.45574	0.01229
9127	P2RX6	0.61151	0.00308	9479	MAPK8IP1	-0.49143	0.00664
9406	ZRANB2	0.43106	0.00312	9487	PIGL	-0.38079	0.01689
9627	SNCAIP	0.47752	0.00965	9695	EDEM1	-0.49969	0.00307
9651	PLCH2	0.88445	0.00197	9896	FIG4	-0.47549	0.00587
10013	HDAC6	0.46770	0.00442	9942	XYLB	-0.56121	0.00074

(continued)

10087	COL4A3BP	0.41511	0.01425	10351	ABCA8	-0.36500	0.00166
10142	AKAP9	0.48875	0.00518	10411	RAPGEF3	-0.48549	0.00122
10699	CORIN	0.46911	0.00765	10485	C1orf61	-0.55889	0.00335
10870	HCST	0.86796	0.00122	10570	DPYSL4	-0.54950	0.00170
10903	MTMR11	0.36712	0.00857	10579	TACC2	-0.41194	0.01235
10984	KCNQ1OT1	0.50755	0.00059	10603	SH2B2	-0.75272	0.00021
11119	BTN3A1	0.66375	0.00478	10629	TAF6L	-0.47736	0.00127
11156	PTP4A3	0.68302	0.00392	10893	MMP24	-0.38591	0.01881
22902	RUFY3	0.35183	0.01314	10924	SMPDL3A	-0.64670	0.00407
23034	SAMD4A	0.53230	0.00612	11178	LZTS1	-0.52217	0.00054
23253	ANKRD12	0.44523	0.00350	11200	CHEK2	-0.40586	0.00679
23378	RRP8	0.47002	0.01194	11248	NXPH3	-0.35645	0.02091
25790	CFAP45	0.42697	0.01011	22821	RASA3	-0.41827	0.01233
25957	PNISR	0.63034	0.00280	23170	TTLL12	-0.52160	0.00581
26047	CNTNAP2	0.53857	0.00492	23387	SIK3	-0.35250	0.01542
26140	TTLL3	0.37152	0.00738	23542	MAPK8IP2	-0.37118	0.01953
26548	ITGB1BP2	0.81476	0.00121	23632	CA14	-0.74370	0.00257
27152	INTU	0.39334	0.01835	23753	SDF2L1	-0.35551	0.00569
27250	PDCD4	0.36145	0.00137	25855	BRMS1	-0.77136	0.00185
27253	PCDH17	0.49747	0.00662	25973	PARS2	-0.35962	0.00622
29015	SLC43A3	0.41372	0.01658	26233	FBXL6	-0.61277	0.00152
29116	MYLIP	0.48371	0.00191	26272	FBXO4	-0.39316	0.01222
49855	SCAPER	0.39255	0.01146	26519	TIMM10	-0.63914	0.00152
51208	CLDN18	0.78341	0.00025	27112	FAM155B	-0.60857	0.00223
51250	C6orf203	0.36034	0.00963	27301	APEX2	-0.53492	0.00748
51334	PRR16	0.49877	0.00823	28988	DBNL	-0.40594	0.00874
51341	ZBTB7A	0.41027	0.00670	29128	UHRF1	-0.44628	0.00996
51554	ACKR4	0.44298	0.00199	29765	TMOD4	-0.43839	0.00328
51710	ZNF44	0.36608	0.01895	29946	SERTAD3	-0.79813	0.00259
54511	HMGCLL1	0.38045	0.00675	30061	SLC40A1	-0.39052	0.00775
54806	AHI1	0.36523	0.00529	30811	HUNK	-0.59851	0.00377
54863	TOR4A	0.38045	0.01237	51207	DUSP13	-0.37917	0.02068
54922	RASIP1	0.38561	0.01583	51550	CINP	-0.40583	0.00408
55035	NOL8	0.36592	0.00602	51734	MSRB1	-0.58463	0.00544
55250	ELP2	0.36848	0.00722	51807	TUBA8	-0.56083	0.00331
55332	DRAM1	0.37135	0.01687	53342	IL17D	-0.61665	0.00236
55450	CAMK2N1	0.54186	0.00336	54606	DDX56	-0.37120	0.00781
55824	PAG1	0.42243	0.01553	54738	FEV	-0.76220	0.00064
55901	THSD1	0.41528	0.01666	54955	C1orf109	-0.55889	0.00287
56100	PCDHGB6	0.82013	0.00032	54974	THG1L	-0.45795	0.01245
56261	GPCPD1	0.55244	0.00067	55199	FAM86C1	-0.65487	0.00087
56311	ANKRD7	0.72027	0.00318	55267	PRR34	-0.59506	0.00660
57139	RGL3	0.56332	0.00172	55357	TBC1D2	-0.36732	0.01086
58484	NLRC4	0.64593	0.00237	55659	ZNF416	-0.54266	0.00493
64114	TMBIM1	0.37832	0.00260	55679	LIMS2	-0.53655	0.00199
79158	GNPTAB	0.38717	0.01350	55783	CMTR2	-0.36330	0.00650
79754	ASB13	0.37325	0.00497	56121	PCDHB15	-0.66916	0.00056
79781	IQCA1	0.46908	0.00858	56931	DUS3L	-0.52755	0.00158
79933	SYNPO2L	0.40423	0.00468	57099	AVEN	-0.45985	0.00298
79962	DNAJC22	0.37050	0.00472	57464	STRIP2	-0.60944	0.00465
80035	ANP32A-IT1	0.45461	0.01160	57529	RGAG1	-0.65137	0.00240
80270	HSD3B7	0.59711	0.00170	57611	ISLR2	-0.37257	0.01281
80298	MTERF2	0.56203	0.00511	57710	KIAA1614	-0.47196	0.00309
80333	KCNIP4	0.46744	0.00939	57716	PRX	-0.48996	0.00521
80726	KIAA1683	0.52742	0.00167	60312	AFAP1	-0.39037	0.00124
80817	CEP44	0.41123	0.00794	63914	LINC01590	-0.65555	0.00262
81691	LOC81691	0.59291	0.00328	63926	ANKEF1	-0.59711	0.00418
81698	LINC00597	0.38561	0.00706	63973	NEUROG2	-0.43501	0.00359
83875	BCO2	0.70697	0.00006	64067	NPAS3	-0.43658	0.01127
83955	NACAP1	0.35029	0.00436	64081	PBLD	-0.70217	0.00194
84081	NSRP1	0.36983	0.02213	64756	ATPAF1	-0.35045	0.01620
84307	ZNF397	0.56121	0.00631	64777	RMND5B	-0.48469	0.00730
84647	PLA2G12B	0.52070	0.00496	64849	SLC13A3	-0.38653	0.00220
84765	ZNF577	0.55187	0.00650	79172	CENPO	-0.43008	0.00173

(continued)

84996	URB1-AS1	0.37149	0.01155	79414	LRFN3	-0.40589	0.01477
116349	EXOC3-AS1	0.53618	0.00241	79624	ARMT1	-0.37057	0.01394
116931	MED12L	0.51322	0.00349	79723	SUV39H2	-0.50500	0.01071
128553	TSHZ2	0.65879	0.00071	79725	THAP9	-0.44918	0.01320
129080	EMID1	0.49877	0.00138	79733	E2F8	-0.74209	0.00131
129530	LYG1	0.43317	0.00777	79810	PTCD2	-0.54546	0.00199
130271	PLEKHH2	0.40702	0.00653	79930	DOK3	-0.67982	0.00126
144132	DNHD1	0.43892	0.01469	80271	ITPKC	-0.47028	0.00166
145226	RDH12	0.38592	0.01675	80781	COL18A1	-0.64595	0.00113
145483	FAM161B	0.54252	0.00137	80818	ZNF436	-0.46884	0.01264
145553	MDP1	0.40568	0.01174	81543	LRRC3	-0.44005	0.00854
145624	PWAR1	0.75677	0.00019	83858	ATAD3B	-0.43819	0.00755
146212	KCTD19	0.54247	0.00257	84182	FAM188B	-0.80820	0.00166
147685	C19orf18	0.38266	0.00064	84254	CAMKK1	-0.35154	0.02197
148418	SAMD13	0.40849	0.00601	84457	PHYHIPL	-0.48325	0.00478
148932	MOB3C	0.43757	0.00473	84465	MEGF11	-0.72027	0.00288
159013	CXorf38	0.38388	0.00982	84657	LINC00852	-0.58146	0.00114
167691	LCA5	0.49131	0.00371	84759	PCGF1	-0.55704	0.00028
169270	ZNF596	0.47764	0.01097	84913	ATOH8	-0.36878	0.00979
196951	FAM227B	0.48723	0.00203	84988	PPP1R16A	-0.57872	0.00140
197257	LDHD	0.68624	0.00245	85443	DCLK3	-0.46995	0.00283
201229	LYRM9	0.82066	0.00083	90024	FLJ20021	-0.61418	0.00578
219347	TMEM254-AS1	0.41372	0.01471	90135	BTBD6	-0.47286	0.00966
221662	RBM24	0.49764	0.00164	90693	CCDC126	-0.58350	0.00550
222389	BEND7	0.36577	0.00177	91582	RPS19BP1	-0.38812	0.01327
254050	LRRC43	0.48772	0.00995	91614	DEPDC7	-0.47894	0.00458
257177	CFAP126	0.86796	0.00130	91734	IDI2	-0.52562	0.00156
280655	IGBP1P1	0.61180	0.00026	112817	HOGA1	-0.57616	0.00334
283011	FLJ37201	0.36702	0.02030	113419	TEX261	-0.36055	0.01412
283106	CSNK2A3	0.36665	0.02207	114034	TOE1	-0.53924	0.00668
283687	ST20-AS1	0.83286	0.00155	114821	ZBED9	-0.36895	0.01183
284942	RPL23AP82	0.45530	0.00945	122616	C14orf79	-0.36732	0.01189
285407	ALG1L9P	0.53834	0.00765	123228	SENP8	-0.65555	0.00330
286184	LINC01289	0.74517	0.00335	124790	HEXIM2	-0.60857	0.00028
340371	NRBP2	0.41182	0.00503	138162	C9orf116	-0.39744	0.01815
342909	ZNF284	0.63375	0.00180	140606	SELM	-0.35547	0.00496
345895	RSPH4A	0.57097	0.00030	140707	BRI3BP	-0.36468	0.01755
375189	PFN4	0.53080	0.00783	144097	C11orf84	-0.35182	0.02126
375248	ANKRD36	0.44084	0.00360	145788	C15orf65	-0.50857	0.00446
387841	RPL13AP20	0.41444	0.00334	147929	ZNF565	-0.74370	0.00168
388115	C15orf52	0.35840	0.01675	150381	PRR34-AS1	-0.44601	0.01270
388327	C17orf100	0.38143	0.00248	151254	ALS2CR11	-0.51422	0.01026
399761	BMS1P5	0.35911	0.01071	151507	MSL3P1	-0.38836	0.00789
400966	RGPD1	0.56959	0.00482	151534	LBX2-AS1	-0.65320	0.00317
401093	MBNL1-AS1	0.48694	0.01081	152877	FAM53A	-0.52630	0.00118
414189	AGAP6	0.37775	0.01048	155060	LOC155060	-0.35504	0.01603
441425	ANKRD20A3	0.59534	0.00460	161882	ZFPM1	-0.36886	0.02234
441430	ANKRD20A2	0.57391	0.00156	171177	RHOV	-0.59412	0.00578
492311	IGIP	0.35213	0.02376	201254	STRA13	-0.40299	0.01168
494551	WEE2	1.32095	0.00054	221150	SKA3	-0.42736	0.00665
574406	ADAMTSL4-AS1	0.54247	0.00570	223082	ZNRF2	-0.42371	0.00341
595135	PGM5P2	0.42447	0.00886	256586	LYSMD2	-0.35577	0.02487
647476	FRG2EP	0.48310	0.00282	257106	ARHGAP30	-0.41590	0.00956
653125	GOLGA8K	0.68642	0.00097	284325	C19orf54	-0.47752	0.00660
654254	ZNF732	0.46350	0.00219	284339	TMEM145	-0.82577	0.00065
677763	SCARNA21	0.55335	0.00607	285463	CTBP1-AS	-0.37625	0.02096
728361	OVOL3	0.61151	0.00502	285847	LOC285847	-0.43226	0.00369
728730	LOC728730	0.88168	0.00083	286140	RNF5P1	-0.43778	0.01351
728963	RPS15AP10	0.59482	0.00309	286257	C9orf142	-0.74037	0.00043
729540	RGPD6	0.35178	0.00472	340393	TMEM249	-0.55507	0.00117
729799	SEC14L1P1	0.36513	0.00677	348110	ARPIN	-0.36932	0.00330
729857	RGPD2	0.54154	0.00196	353174	ZACN	-0.42376	0.01527
790953	TSL	0.53493	0.00602	374383	NCR3LG1	-0.47461	0.00162
100128239	LOC100128239	0.53228	0.00857	377007	KLHL30	-0.43923	0.00518

(continued)

100129195	ZSCAN16-AS1	0.39682	0.00025	389119	FAM212A	-0.44479	0.01155
100130733	LRRC70	0.79817	0.00012	391712	TRIM61	-0.49026	0.00732
100132781	LOC100132781	0.51121	0.00193	400236	FOXN3-AS1	-0.59761	0.00404
100133991	MAP3K14-AS1	0.48201	0.00894	400566	C17orf97	-1.11630	0.00033
100169989	DBIL5P2	0.52070	0.00986	401509	ZNF658B	-0.35421	0.00158
100302692	FTX	0.35126	0.02500	402682	UFSP1	-0.65160	0.00070
100379224	LOC100379224	0.51606	0.00519	414778	HCG17	-0.37075	0.02098
100381270	ZBED6	0.46461	0.00069	440503	PLIN5	-0.48298	0.00788
100505832	PROX1-AS1	0.43622	0.01216	550112	UBA6-AS1	-0.36702	0.01341
100506023	LOC100506023	0.43622	0.01037	554235	ASPDH	-0.43226	0.00864
100506472	LOC100506472	0.51924	0.00688	641451	SNORA19	-0.68511	0.00082
100506801	LOC100506801	0.38391	0.01152	645206	LINC00693	-0.46908	0.00609
100507401	LRP4-AS1	0.43879	0.00180	647121	EMBP1	-0.67828	0.00315
100507547	LOC100507547	0.74677	0.00075	647310	TEX22	-0.78354	0.00085
100526820	CAHM	0.57945	0.00547	653653	LOC653653	-0.42168	0.00685
100534595	HNRNPUL2-BSCL2	0.38907	0.01498	728039	SSR4P1	-0.50972	0.00424
100874110	GLYCTK-AS1	0.48272	0.00798	729665	CCDC175	-0.53830	0.00570
100874291	ALMS1-IT1	0.48568	0.00647	100129518	LOC100129518	-0.48549	0.00023
100874392	ANKRD20A12P	0.72005	0.00043	100130958	SYCE1L	-0.42269	0.00393
100996511	LINC01355	0.41480	0.00651	100131655	LOC100131655	-1.01040	0.00027
101926911	LOC101926911	0.37832	0.01444	100144748	KLLN	-0.67825	0.00244
101927492	UTAT33	0.43896	0.00682	100303491	ZEB2-AS1	-0.46549	0.00394
101928053	LOC101928053	0.49723	0.01107	100507291	LOC100507291	-0.43226	0.00757
101928539	LOC101928539	0.46350	0.01285	100507299	SMC5-AS1	-0.41590	0.01108
101929215	CTD-2201I18.1	0.46350	0.00544	100652748	TIMM23B	-0.41553	0.00042
101929680	LOC101929680	0.42388	0.00676	101928378	PTOV1-AS2	-0.45889	0.00633
101929717	LOC101929717	0.59459	0.00313	101928841	LOC101928841	-0.65137	0.00291
101929746	ZNF341-AS1	0.42697	0.00935	101929074	PIK3CD-AS2	-0.42858	0.00038
101930010	LOC101930010	0.37530	0.00887	104355295	SGMS1-AS1	-0.41598	0.00337
102723513	ZNF30-AS1	0.56345	0.00602	104472717	LINC01224	-0.40338	0.01122
103625684	RNU6-2	-0.16854	0.44304				

Table 1. Selected DEG list based on the Quant-mRNA sequencing result

UP regulated Gene Ontology			
Term		Count	Pvalue
GO:0007155	cell adhesion	32	0.00276
GO:0022610	biological adhesion	32	0.00291
GO:0061061	muscle structure development	13	0.02755
GO:0046649	lymphocyte activation	13	0.04843
GO:0007517	muscle organ development	10	0.01888
GO:0001558	regulation of cell grow th	10	0.03234
GO:0098742	cell-cell adhesion via plasma-membrane adhesion molecules	9	0.00362
GO:0048871	multicellular organismal homeostasis	9	0.02279
GO:0016042	lipid catabolic process	8	0.04194
GO:0032409	regulation of transporter activity	7	0.02428
GO:1904062	regulation of cation transmembrane transport	7	0.02909
GO:0048771	tissue remodeling	6	0.02059
GO:0007156	homophilic cell adhesion via plasma membrane adhesion molecules	6	0.02991
GO:0002028	regulation of sodium ion transport	5	0.01275
GO:0051250	negative regulation of lymphocyte activation	5	0.04418
GO:0000042	protein targeting to Golgi	4	0.00126
GO:0072600	establishment of protein localization to Golgi	4	0.00191
GO:0000301	retrograde transport, vesicle recycling w ithin Golgi	4	0.00273
GO:0010765	positive regulation of sodium ion transport	4	0.00641
GO:0034067	protein localization to Golgi apparatus	4	0.00693
GO:0006891	intra-Golgi vesicle-mediated transport	4	0.01614
GO:1902305	regulation of sodium ion transmembrane transport	4	0.01989
GO:0034103	regulation of tissue remodeling	4	0.03785
GO:1902307	positive regulation of sodium ion transmembrane transport	3	0.01780
GO:1901385	regulation of voltage-gated calcium channel activity	3	0.03938
GO:0042462	eye photoreceptor cell development	3	0.04980
GO:0043316	cytotoxic T cell degranulation	2	0.02162
DOWN regulated Gene Ontology			
Term		Count	Pvalue
GO:0034654	nucleobase-containing compound biosynthetic process	66	0.04331
GO:0006355	regulation of transcription, DNA-templated	56	0.04432
GO:1903506	regulation of nucleic acid-templated transcription	56	0.04894
GO:0031327	negative regulation of cellular biosynthetic process	30	0.00831
GO:0009890	negative regulation of biosynthetic process	30	0.01026
GO:0045934	negative regulation of nucleobase-containing compound metabolic process	29	0.00551
GO:0010558	negative regulation of macromolecule biosynthetic process	29	0.00859
GO:0051172	negative regulation of nitrogen compound metabolic process	29	0.01815
GO:1903507	negative regulation of nucleic acid-templated transcription	28	0.00129
GO:1902679	negative regulation of RNA biosynthetic process	28	0.00159
GO:0051253	negative regulation of RNA metabolic process	28	0.00271
GO:2000113	negative regulation of cellular macromolecule biosynthetic process	26	0.02125
GO:0045892	negative regulation of transcription, DNA-templated	25	0.00634
GO:0051276	chromosome organization	23	0.03487
GO:0006259	DNA metabolic process	22	0.01120
GO:0051241	negative regulation of multicellular organismal process	20	0.04597
GO:0044712	single-organism catabolic process	19	0.01543
GO:0051093	negative regulation of developmental process	18	0.01002
GO:0000122	negative regulation of transcription from RNA polymerase II promoter	18	0.01120
GO:0006325	chromatin organization	18	0.01421
GO:0051270	regulation of cellular component movement	18	0.02077
GO:0030334	regulation of cell migration	17	0.01078
GO:2000145	regulation of cell motility	17	0.01994
GO:0040012	regulation of locomotion	17	0.02818
GO:0006974	cellular response to DNA damage stimulus	17	0.04139
GO:0045596	negative regulation of cell differentiation	15	0.02723

(continued)

GO:0071363	cellular response to grow th factor stimulus	14	0.03902
GO:0008610	lipid biosynthetic process	14	0.04536
GO:0006281	DNA repair	13	0.03117
GO:0044089	positive regulation of cellular component biogenesis	12	0.02094
GO:0048514	blood vessel morphogenesis	12	0.04099
GO:0002683	negative regulation of immune system process	11	0.02223
GO:0001525	angiogenesis	11	0.03221
GO:0051090	regulation of sequence-specific DNA binding transcription factor activity	10	0.04170
GO:0051235	maintenance of location	9	0.02739
GO:0006260	DNA replication	9	0.02739
GO:1903707	negative regulation of hemopoiesis	8	0.00148
GO:0016458	gene silencing	8	0.03738
GO:0006261	DNA-dependent DNA replication	7	0.00916
GO:0046395	carboxylic acid catabolic process	7	0.03292
GO:0045017	glycerolipid biosynthetic process	7	0.03966
GO:0006643	membrane lipid metabolic process	7	0.04068
GO:0030336	negative regulation of cell migration	7	0.04946
GO:1904019	epithelial cell apoptotic process	6	0.00485
GO:0045638	negative regulation of myeloid cell differentiation	6	0.00584
GO:0006342	chromatin silencing	6	0.01590
GO:0009163	nucleoside biosynthetic process	6	0.02174
GO:1901659	glycosyl compound biosynthetic process	6	0.02306
GO:0045814	negative regulation of gene expression, epigenetic	6	0.02656
GO:0043433	negative regulation of sequence-specific DNA binding transcription factor activity	6	0.02731
GO:0051262	protein tetramerization	6	0.02806
GO:0090101	negative regulation of transmembrane receptor protein serine/threonine kinase signaling pathw ay	5	0.04201
GO:2000209	regulation of anoikis	4	0.00346
GO:0043276	anoikis	4	0.00480
GO:0061641	CENP-A containing chromatin organization	4	0.01581
GO:0034080	CENP-A containing nucleosome assembly	4	0.01581
GO:1904837	beta-catenin-TCF complex assembly	4	0.01682
GO:0030219	megakaryocyte differentiation	4	0.01894
GO:0030514	negative regulation of BMP signaling pathw ay	4	0.02005
GO:0031055	chromatin remodeling at centromere	4	0.02005
GO:0036297	interstrand cross-link repair	4	0.02360
GO:0006336	DNA replication-independent nucleosome assembly	4	0.02882
GO:0034508	centromere complex assembly	4	0.02882
GO:0034724	DNA replication-independent nucleosome organization	4	0.03022
GO:0043486	histone exchange	4	0.03614
GO:0001885	endothelial cell development	4	0.03614
GO:0002260	lymphocyte homeostasis	4	0.03771
GO:0051965	positive regulation of synapse assembly	4	0.04262
GO:2000210	positive regulation of anoikis	3	0.00402
GO:0010866	regulation of triglyceride biosynthetic process	3	0.01817
GO:0045653	negative regulation of megakaryocyte differentiation	3	0.02028
GO:0031297	replication fork processing	3	0.04624
GO:0045652	regulation of megakaryocyte differentiation	3	0.04928
GO:0042036	negative regulation of cytokine biosynthetic process	3	0.04928
GO:0038098	sequestering of BMP from receptor via BMP binding	2	0.03649

Table 2. Gene ontology lists based on searches done by DAVID

UP regulated KEGG pathway			
Term		Count	PValue
hsa05322	Systemic lupus erythematosus	17	1.4658E-04
hsa04080	Neuroactive ligand-receptor interaction	24	1.3474E-03
hsa04020	Calcium signaling pathway	18	1.3656E-03
hsa05146	Amoebiasis	13	1.5737E-03
hsa05150	Staphylococcus aureus infection	9	1.7263E-03
hsa04621	NOD-like receptor signaling pathway	9	1.9479E-03
hsa05144	Malaria	8	4.1041E-03
hsa04610	Complement and coagulation cascades	9	8.0538E-03
hsa04976	Bile secretion	9	8.0538E-03
hsa04640	Hematopoietic cell lineage	10	9.1376E-03
hsa04970	Salivary secretion	10	9.8406E-03
hsa04514	Cell adhesion molecules (CAMs)	13	1.6277E-02
hsa04512	ECM-receptor interaction	9	2.9499E-02
hsa05323	Rheumatoid arthritis	9	3.1312E-02
hsa00120	Primary bile acid biosynthesis	4	3.2431E-02
hsa05332	Graft-versus-host disease	5	4.8276E-02
hsa05321	Inflammatory bowel disease (IBD)	7	5.1551E-02
hsa04151	PI3K-Akt signaling pathway	22	5.5882E-02
hsa05200	Pathways in cancer	24	6.6043E-02
hsa05034	Alcoholism	13	6.9633E-02
hsa04974	Protein digestion and absorption	8	7.6665E-02
hsa04975	Fat digestion and absorption	5	7.9992E-02
hsa05416	Viral myocarditis	6	9.0728E-02
hsa04940	Type I diabetes mellitus	5	9.8912E-02
DOWN regulated KEGG pathway			
Term		Count	PValue
hsa04974	Protein digestion and absorption	7	1.9239E-04
hsa05322	Systemic lupus erythematosus	7	1.7995E-03
hsa05034	Alcoholism	6	2.8047E-02
hsa04512	ECM-receptor interaction	5	9.8370E-03

Table 3. KEGG pathway lists based on searches done by DAVID

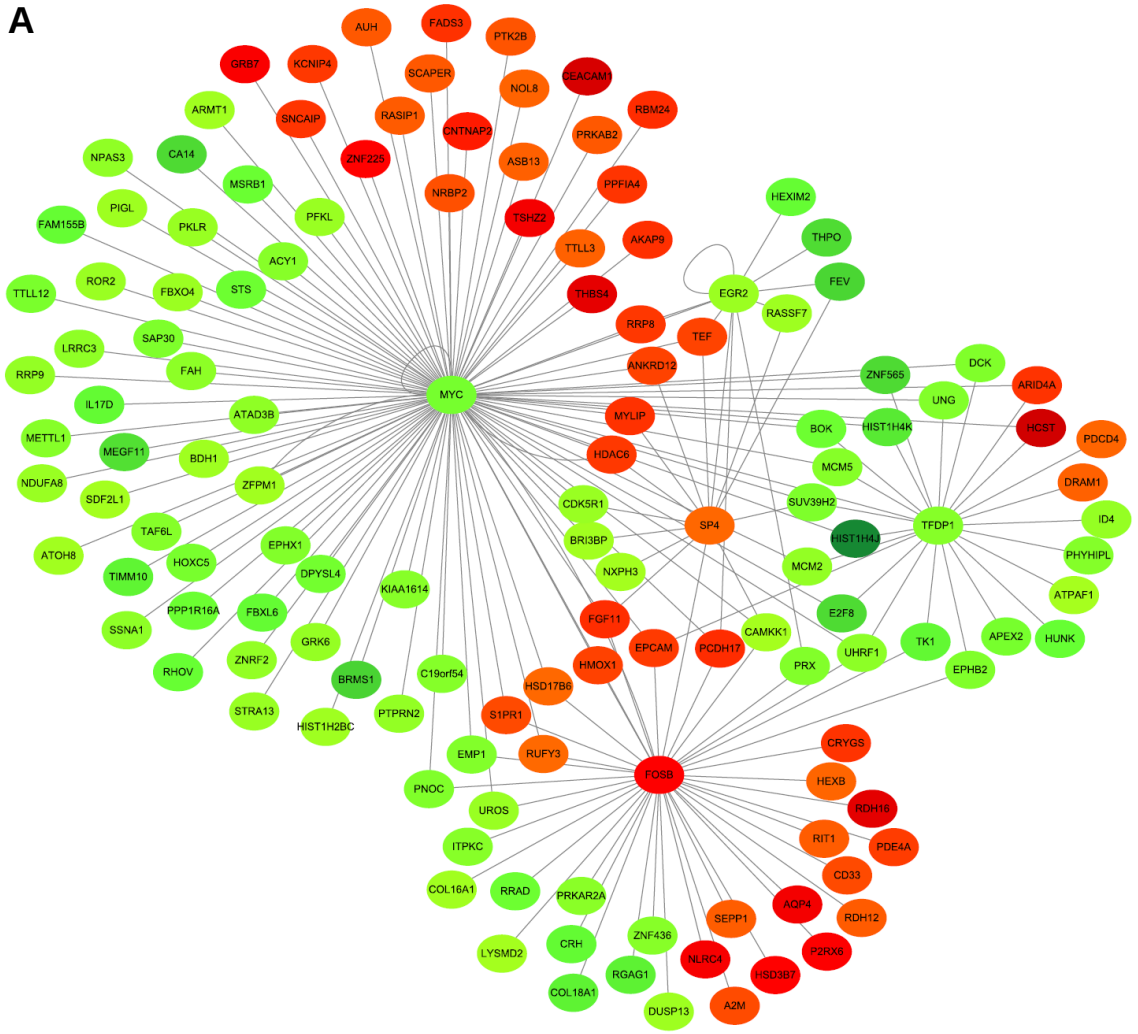
A
AUH
FADS3
PTK2B
GRB7
KCNIP4
SCAPER
NOL8
CEACAM1
ARMT1
SNCAIP
RASIP1
RBM24
CNTNAP2
PRKAB2
NPAS3
CA14
ZNF225
ASB13
MSRB1
NRBP2
PPFIA4
HEXIM2
PIGL
PFKL
TSHZ2
THPO
FAM155B
PKLR
TTLL3
AKAP9
ACY1
FEV
TTLL12
ROR2
FBXO4
STS
THBS4
EGR2
RASSF7
RRP8
TEF
SAP30
LRRC3
ANKRD12
ZNF565
DCK
RRP9
FAH
MYC
ARID4A
IL17D
ATAD3B
MYLIP
UNG
BOK
HIST1H4K
HCST
METTL1
MEGF11
BDH1
HDAC6
PDCD4
MCM5
NDUFA8
ZFPM1
DRAM1
SDF2L1
CDK5R1
SUV39H2
ID4
TAF6L
SP4
TFDP1
BRI3BP
HIST1H4J
ATOH8
EPHX1
HOXC5
NXPH3
MCM2
PHYHIPL
TIMM10
DPYSL4
KIAA1614
E2F8
ATPAF1
PPP1R16A
FBXL6
FGF11
CAMKK1
SSNA1
GRK6
EPCAM
PCDH17
TK1
APEX2
HUNK
ZNRF2
UHRF1
RHOV
HMOX1
PRX
EPHB2
BRMS1
C19orf54
HSD17B6
STRA13
PTPRN2
S1PR1
HIST1H2BC
CRYGS
EMP1
RUFY3
FOSB
HEXB
PNOC
RDH16
UROS
RIT1
PDE4A
ITPKC
CD33
COL16A1
RRAD
PRKAR2A
AQP4
SEPP1
RDH12
ZNF436
LYSMD2
CRH
NLRC4
PZRX6
RGAG1
HSD3B7
COL18A1
DUSP13
A2M
B
UP-regulated
17%
15%
8%
60%
Transcriptional regulation
Cytoskeleton
Immune-related
Other
DOWN-regulated
15%
12%
8%
7%
58%
Transcriptional regulation
Histone modification
Cytoskeleton
Mitochondria
Other

Figure 10. Selected genes and analyzed data based on the RNA sequencing result

(A) Cytoscape map showing interactions between transcription factors and their target genes. Red means up-regulated and green means down-regulated. Color intensity indicates the fold change of each gene. DEGs were selected for the analysis based on $p<0.05$, $|\log_2 FC|<0.35$. (B) Pie charts depicting the proportion of genes associated with transcriptional regulation, histone modification, cytoskeleton, immune response, and mitochondria altered in aged-V40G αSyn treated cells.

Genes regulated by MYC			
Entrez ID	**Gene**	**Protein**	**FC**
10870	HCST	Hematopoietic cell signal transducer	0.86796
634	CEACAM1	Carcinoembryonic antigen-related cell adhesion molecule 1	0.83331
7060	THBS4	Thrombospondin-4	0.74871
128553	TSHZ2	Teashirt homolog 2	0.65879
2886	GRB7	Grow th factor receptor-bound protein 7	0.63207
7768	ZNF225	Zinc finger protein 225	0.59846
26047	CNTNAP2	Contactin-associated protein-like 2	0.53857
221662	RBM24	RNA-binding protein 24	0.49764
27253	PCDH17	Protocadherin-17	0.49747
2256	FGF11	Fibroblast grow th factor 11	0.49353
10142	AKAP9	A-kinase anchor protein 9	0.48875
3995	FADS3	Fatty acid desaturase 3	0.48566
29116	MYLIP	E3 ubiquitin-protein ligase MYLIP	0.48371
5926	ARID4A	AT-rich interactive domain-containing protein 4A	0.48061
9627	SNCAIP	Synphilin-1	0.47752
8497	PPFIA4	Liprin-alpha-4	0.47665
23378	RRP8	Ribosomal RNA-processing protein 8	0.47002
10013	HDAC6	Histone deacetylase 6	0.46770
80333	KCNIP4	Kv channel-interacting protein 4	0.46744
4072	EPCAM	Epithelial cell adhesion molecule	0.46350
3162	HMOX1	Heme oxygenase 1	0.44734
23253	ANKRD12	Ankyrin repeat domain-containing protein 12	0.44523
7008	TEF	Transcriptional enhancer factor TEF-1	0.44252
1901	S1PR1	Sphingosine 1-phosphate receptor 1	0.42697
340371	NRBP2	Nuclear receptor-binding protein 2	0.41182
2185	PTK2B	Protein-tyrosine kinase 2-beta	0.40189
5565	PRKAB2	5'-AMP-activated protein kinase subunit beta-2	0.39350
49855	SCAPER	S phase cyclin A-associated protein in the endoplasmic reticulum	0.39255
549	AUH	Methylglutaconyl-CoA hydratase, mitochondrial	0.39205
54922	RASIP1	Ras-interacting protein 1	0.38561
79754	ASB13	Ankyrin repeat and SOCS box protein 13	0.37325
26140	TTLL3	Tubulin monoglycylase TTLL3	0.37152
55035	NOL8	Nucleolar protein 8	0.36592
8630	HSD17B6	17-beta-hydroxysteroid dehydrogenase type 6	0.35427
22902	RUFY3	Protein RUFY3	0.35183
8363	HIST1H4J	Histone cluster 1 H4 family member J	-1.06827
25855	BRMS1	Breast cancer metastasis-suppressor 1	-0.77136
23632	CA14	Carbonic anhydrase 14	-0.74370
147929	ZNF565	Zinc finger protein 565	-0.74370
79733	E2F8	Transcription factor E2F8	-0.74209
84465	MEGF11	Multiple epidermal grow th factor-like domains protein 11	-0.72027
8362	HIST1H4K	Histone cluster 1 H4 family member K	-0.68308
26519	TIMM10	Mitochondrial import inner membrane translocase subunit Tim10	-0.63914
53342	IL17D	Interleukin-17D	-0.61665
26233	FBXL6	F-box/LRR-repeat protein 6	-0.61277
27112	FAM155B	Transmembrane protein FAM155B	-0.60857
171177	RHOV	Rho-related GTP-binding protein RhoV	-0.59412
51734	MSRB1	Methionine-R-sulfoxide reductase B1	-0.58463
84988	PPP1R16A	Protein phosphatase 1 regulatory subunit 16A	-0.57872
412	STS	Steryl-sulfatase	-0.57254
666	BOK	Bcl-2-related ovarian killer protein	-0.57185
10570	DPYSL4	Dihydropyrimidinase-related protein 4	-0.54950
3222	HOXC5	Homeobox protein Hox-C5	-0.53133
23170	TTLL12	Tubulin--tyrosine ligase-like protein 12	-0.52160
8819	SAP30	Histone deacetylase complex subunit SAP30	-0.50731
79723	SUV39H2	Histone-lysine N-methyltransferase SUV39H2	-0.50500
5368	PNOC	Prepronociceptin	-0.49859
1633	DCK	Deoxycytidine kinase	-0.49656
7374	UNG	Uracil-DNA glycosylase	-0.49065
2012	EMP1	Epithelial membrane protein 1	-0.49026
2052	EPHX1	Epoxide hydrolase 1	-0.48938
10629	TAF6L	TAF6-like RNA polymerase II p300/CBP-associated factor-associated factor 65 kDa subunit 6L	-0.47736
4174	MCM5	DNA replication licensing factor MCM5	-0.47494
95	ACY1	Aminoacylase-1	-0.47160
2184	FAH	Fumarylacetoacetase	-0.44735
29128	UHRF1	E3 ubiquitin-protein ligase UHRF1	-0.44628
8636	SSNA1	Sjoegren syndrome nuclear autoantigen 1	-0.44280
81543	LRRC3	Leucine-rich repeat-containing protein 3	-0.44005
83858	ATAD3B	ATPase family AAA domain-containing protein 3B	-0.43819
64067	NPAS3	Neuronal PAS domain-containing protein 3	-0.43658
4171	MCM2	DNA replication licensing factor MCM2	-0.42434
223082	ZNRF2	E3 ubiquitin-protein ligase ZNRF2	-0.42371
5799	PTPRN2	Receptor-type tyrosine-protein phosphatase N2	-0.42200

(continued)

9136	RRP9	U3 small nucleolar RNA-interacting protein 2	-0.41984
2870	GRK6	G protein-coupled receptor kinase 6	-0.41391
5313	PKLR	Pyruvate kinase PKLR	-0.40385
201254	STRA13	Centromere protein X	-0.40299
7390	UROS	Uroporphyrinogen-III synthase	-0.40143
5211	PFKL	ATP-dependent 6-phosphofructokinase, liver type	-0.40055
4702	NDUFA8	NADH dehydrogenase [ubiquinone] 1 alpha subcomplex subunit 8	-0.40009
8851	CDK5R1	Cyclin-dependent kinase 5 activator 1	-0.39892
4920	ROR2	Tyrosine-protein kinase transmembrane receptor ROR2	-0.39799
26272	FBXO4	F-box only protein 4	-0.39316
9487	PIGL	N-acetylglucosaminyl-phosphatidylinositol de-N-acetylase	-0.38079
622	BDH1	D-beta-hydroxybutyrate dehydrogenase, mitochondrial	-0.37801
8347	HIST1H2BC	Histone H2B type 1-C/E/F/G/I	-0.37580
79624	ARMT1	Protein-glutamate O-methyltransferase	-0.37057
161882	ZFPM1	Zinc finger protein ZFPM1	-0.36886
140707	BRI3BP	BRI3-binding protein	-0.36468
23753	SDF2L1	Stromal cell-derived factor 2-like protein 1	-0.35551
84254	CAMKK1	Calcium/calmodulin-dependent protein kinase kinase 1	-0.35154
Genes regulated by FOSB			
Entrez ID	**Gene**	**Protein**	**FC**
8608	RDH16	Retinol dehydrogenase 16	0.7559
361	AQP4	Aquaporin-4	0.6647
58484	NLRC4	NLR family CARD domain-containing protein 4	0.6459
9127	P2RX6	P2X purinoceptor 6	0.6115
80270	HSD3B7	3 beta-hydroxysteroid dehydrogenase type 7	0.5971
27253	PCDH17	Protocadherin-17	0.4975
2256	FGF11	Fibroblast grow th factor 11	0.4935
1427	CRYGS	Beta-crystallin S	0.4792
4072	EPCAM	Epithelial cell adhesion molecule	0.4635
5141	PDE4A	cAMP-specific 3',5'-cyclic phosphodiesterase 4A	0.4578
3162	HMOX1	Heme oxygenase 1	0.4473
1901	S1PR1	Sphingosine 1-phosphate receptor 1	0.4270
945	CD33	Myeloid cell surface antigen CD33	0.4270
2	A2M	Alpha-2-macroglobulin	0.4229
145226	RDH12	Retinol dehydrogenase 12	0.3859
6016	RIT1	GTP-binding protein Rit1	0.3841
6414	SEPP1	Selenoprotein P	0.3801
3074	HEXB	Beta-hexosaminidase subunit beta	0.3616
8630	HSD17B6	17-beta-hydroxysteroid dehydrogenase type 6	0.3543
22902	RUFY3	Protein RUFY3	0.3518
7083	TK1	Thymidine kinase, cytosolic	-0.6226
1392	CRH	Corticotropin-releasing factor receptor 2	-0.6161
6236	RRAD	GTP-binding protein RAD	-0.5719
5368	PNOC	Prepronociceptin	-0.4986
2012	EMP1	Epithelial membrane protein 1	-0.4903
29128	UHRF1	E3 ubiquitin-protein ligase UHRF1	-0.4463
7390	UROS	Uroporphyrinogen-III synthase	-0.4014
84254	CAMKK1	Calcium/calmodulin-dependent protein kinase kinase 1	-0.3515

Table 4. Gene lists regulated by transcription factors, MYC and FOSB

by related mechanism and revealed selective changes in the expression of transcriptional regulation, histone modification, cytoskeleton organization, immune response, and mitochondria-related mechanism (Figure 10B). These selective changes of gene expression level suggest that aged αSyn communicates with the cellular gene expression machinery, and this may point toward the increase of pathology-specific mechanisms like the cell-to-cell transmission of αSyn aggregates.

With all, simplified scheme was drawn illustrating about the persuasive procedure of alteration in intracellular vesicle trafficking by extracellular aged αSyn (Figure 11). In response to extracellular aged αSyn, changes on histone modification and transcriptional regulation might induce some alterations in cytoskeleton organization, immune response and mitochondria mechanism. These changes seem to make vesicles bypass the endo-lysosomal pathway and lead to cell-to-cell transmission increase. For confirmation, it might be necessary to study whether MYC overexpression could show inhibitory effect on transcellular transmission. The further studies for establishing mechanism network of cell-to-cell αSyn transmission would contribute to understanding the specific mechanism of pathogenic protein aggregate propagation on several neurodegenerative diseases.

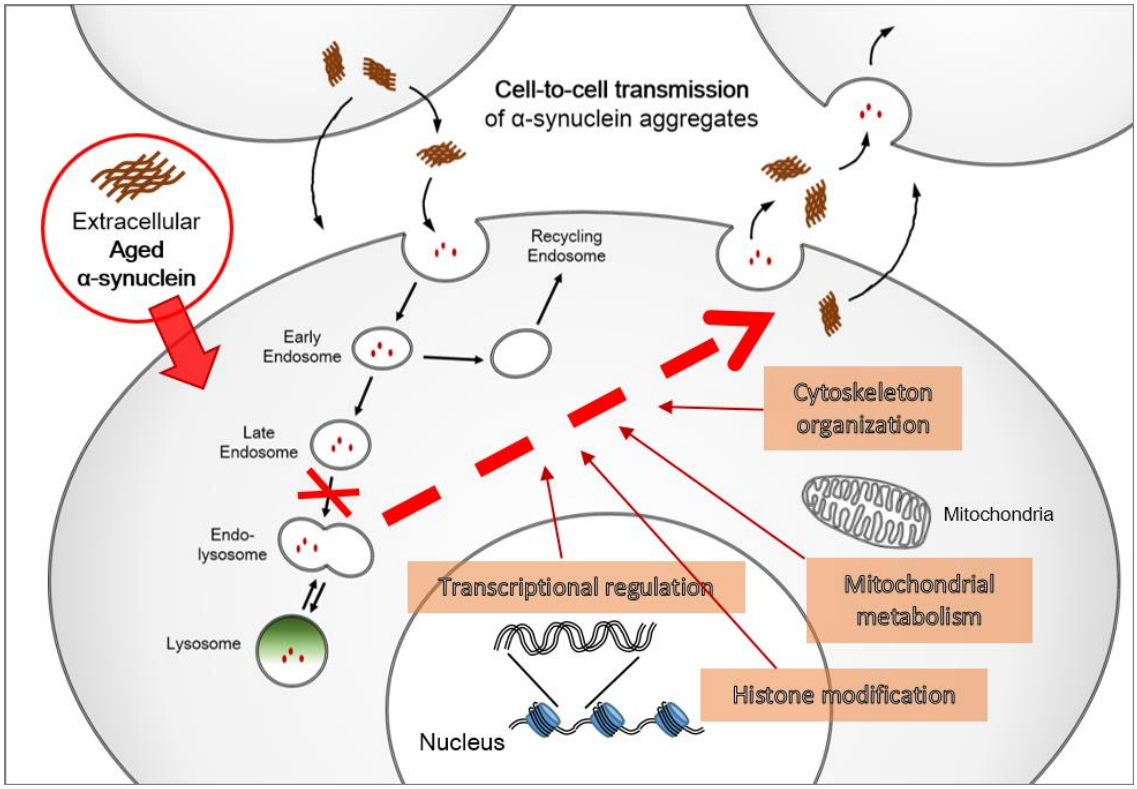

Figure 11. Simplified scheme illustrating increased αSyn transmission by extracellular aged αSyn

Changes in several cellular mechanisms by extracellular aged αSyn induce the reduction of endo-lysosomal degradation rate. And this results in the cell-to-cell αSyn transmission increase.

DISCUSSION

Herein, I investigated the question as to whether the template seeding is the underlying mechanism of αSyn aggregate propagation. I used WT αSyn and V40G variant of αSyn; the latter lacks the seeding ability. When neuronal cells were treated with fresh or aged αSyn of WT and V40G, I found that αSyn aggregate transmission level was increased not only in the aged-WT treated condition but also in aged-V40G treated condition. If αSyn aggregate transmission is mainly dependent on the seeding ability, it would be shown increased aggregate transmission level only in the aged-WT treated condition. From the result, I conclude that the template seeding is not the principal mechanism of αSyn aggregates propagation.

In some studies, they showed that other factors appear to be involved in the induction and spreading of αSyn pathology. Injection of αSyn lacking NAC region which is associated with aggregation and Lewy body formation was sufficient to form αSyn pathology in neocortex and hippocampus [46, 47]. In addition, lipopolysaccharides (LPS) injection into substantia nigra of the αSyn transgenic mice formed αSyn inclusion and dopaminergic neuron loss as well as massive inflammatory reactions [48]. Correlated with this, injection of anti-inflammatory agent resulted in reducing the degree of disease progression [49]. Recently, the body of papers focusing on this inflammatory reaction in PD is growing bigger. αSyn fibril exposure in the rat brain provoked major histocompatibility complex II (MHC II) response and caused the recruitment of monocytes in the striatum prior to neurodegeneration [50]. αSyn aggregates drove cytotoxic and helper T cell responses in PD patients acting as antigen

[51]. Aiming at downregulation of inflammatory processes might be important to slow down the progression of PD [52, 53]. Also, one of the pesticides, rotenone, caused high nigrostriatal dopaminergic degeneration by inhibition of mitochondrial complex I [54]. These also support that the template seeding is not the principal mechanism of αSyn aggregates transmission and LBs pathology propagation.

Other factors might be involved in increasing αSyn aggregate transmission such as impairment of intracellular protein homeostasis by the failure of proteasome, autophagosome, and lysosome, all of which may be caused by an aggregate form of αSyn itself. To verify what mechanism is really happens by extracellular αSyn aggregates and leads to increase of αSyn aggregate transmission, several tests were conducted in this study. Through the immunoblot analysis, there was no changes in selective autophagy pathway and biosynthetic pathway. This indicates that decreased misfolded protein degradation or increased secretion is not the reason of αSyn aggregate transmission increase. But alteration in the endo-lysosomal degradation pathway by aged αSyn was observed via fluorescein-conjugated dextran degradation test. Based on this result, another immunoblot analysis and cell imaging were performed to identify whether the lysosome status is intact. According to results of galectin-3 puncta assay, immunoblot of lysosomal hydrolases, and lysotracker red staining, there was no effect of aged αSyn on lysosome status. Therefore, bypassing the fusion with lysosomes in the endo-lysosomal degradation pathway could be hypothesized as an effect of extracellular aged αSyn in cells. This hypothesis followed by the increase of protein level in cells and aggregate formation, resulting in increased αSyn aggregate transmission.

It was hard to find the causative factor by checking each part of intracellular mechanisms one by one. Thereby it was necessary to change the way to narrow down the range of candidates. So RNA sequencing was conducted. RNA-seq result showed that there were gene expression level changes related in transcriptional regulation, immune response, cytoskeleton organization, and mitochondrial mechanism. Recently other studies performed transcriptome to find causative factors in PD. Transcriptome analysis of PD patients derived dopaminergic neurons showed elevated RBFOX1, a splicing factor, leading oxidative stress vulnerability by dysregulation of mitochondrial genes [55]. Genes related to RNA and DNA production, mitochondria metabolism, protein folding system and particularly the GABAergic neurotransmission significantly enriched in the brain tissue of DLB patients [56]. Meta-analysis of PD transcriptome data of whole substantia nigra tissue and microdissected dopaminergic neurons showed up-regulated inflammation specific genes [57]. Using a patient-specific induced pluripotent stem cell (iPSC)-based dopaminergic neurons (DAn) model, extensive DNA methylation changes, and of RNA expression which commonly shown in LRRK2-associated PD and sporadic PD [58]. Profile of the iPSC-derived DAn, purified from PD patients carrying LRRK2 G2019S variants, was matched with Parkinsonian neurotoxin rotenone induced expression changes [59].

Based on such transcriptome results, understanding of the detailed mechanisms about how expression level changed genes work in the αSyn aggregate transmission is needed as further studies. Establishing the network map of each related intracellular mechanism inducing αSyn aggregate transmission increase is also needed. This will be able to clarify the mechanism in the αSyn aggregate transmission,

leading to the LBs or LNs development and propagation in PD. Furthermore, it will be able to find potent therapeutic target reducing the αSyn aggregate transmission and progression of PD.

In conclusion, the template seeding is not the principal mechanism of αSyn aggregate transmission and LBs pathology propagation in PD. Instead, extracellular aged αSyn make changes in several gene expression related to transcriptional regulation, immune response, cytoskeleton organization, and mitochondrial mechanism. These changes bring the reduction of endo-lysosomal degradation, leading to increased intracellular αSyn aggregate transmission.

REFERENCES

1. Braak, H., et al., *Staging of brain pathology related to sporadic Parkinson's disease.* Neurobiol Aging, 2003. **24**(2): p. 197-211.
2. Jellinger, K.A., *A critical reappraisal of current staging of Lewy-related pathology in human brain.* Acta Neuropathol, 2008. **116**(1): p. 1-16.
3. Lashuel, H.A., et al., *The many faces of alpha-synuclein: from structure and toxicity to therapeutic target.* Nat Rev Neurosci, 2013. **14**(1): p. 38-48.
4. Crowther, R.A., S.E. Daniel, and M. Goedert, *Characterisation of isolated alpha-synuclein filaments from substantia nigra of Parkinson's disease brain.* Neurosci Lett, 2000. **292**(2): p. 128-30.
5. Spillantini, M.G., et al., *Filamentous alpha-synuclein inclusions link multiple system atrophy with Parkinson's disease and dementia with Lewy bodies.* Neurosci Lett, 1998. **251**(3): p. 205-8.
6. Brettschneider, J., et al., *Spreading of pathology in neurodegenerative diseases: a focus on human studies.* Nat Rev Neurosci, 2015. **16**(2): p. 109-20.
7. Jucker, M. and L.C. Walker, *Self-propagation of pathogenic protein aggregates in neurodegenerative diseases.* Nature, 2013. **501**(7465): p. 45-51.
8. Oueslati, A., M. Ximerakis, and K. Vekrellis, *Protein Transmission, Seeding and Degradation: Key Steps for alpha-Synuclein Prion-Like Propagation.* Exp Neurobiol, 2014. **23**(4): p. 324-36.
9. Chiti, F. and C.M. Dobson, *Protein misfolding, functional amyloid, and human disease.* Annu Rev Biochem, 2006. **75**: p. 333-66.

10. Spillantini, M.G., et al., *alpha-Synuclein in filamentous inclusions of Lewy bodies from Parkinson's disease and dementia with lewy bodies.* Proc Natl Acad Sci U S A, 1998. **95**(11): p. 6469-73.

11. Chartier-Harlin, M.C., et al., *Alpha-synuclein locus duplication as a cause of familial Parkinson's disease.* Lancet, 2004. **364**(9440): p. 1167-9.

12. Ibanez, P., et al., *Causal relation between alpha-synuclein gene duplication and familial Parkinson's disease.* Lancet, 2004. **364**(9440): p. 1169-71.

13. Singleton, A.B., et al., *alpha-Synuclein locus triplication causes Parkinson's disease.* Science, 2003. **302**(5646): p. 841.

14. Springer, W. and P.J. Kahle, *Mechanisms and models of alpha-synuclein-related neurodegeneration.* Curr Neurol Neurosci Rep, 2006. **6**(5): p. 432-6.

15. Guo, J.L. and V.M. Lee, *Cell-to-cell transmission of pathogenic proteins in neurodegenerative diseases.* Nat Med, 2014. **20**(2): p. 130-8.

16. Lee, S.J., et al., *Cell-to-cell transmission of non-prion protein aggregates.* Nat Rev Neurol, 2010. **6**(12): p. 702-6.

17. Brundin, P., R. Melki, and R. Kopito, *Prion-like transmission of protein aggregates in neurodegenerative diseases.* Nat Rev Mol Cell Biol, 2010. **11**(4): p. 301-7.

18. Danzer, K.M., et al., *Exosomal cell-to-cell transmission of alpha synuclein oligomers.* Molecular Neurodegeneration, 2012. **7**(1): p. 42.

19. Desplats, P., et al., *Inclusion formation and neuronal cell death through neuron-to-neuron transmission of alpha-synuclein.* Proc Natl Acad Sci U S A, 2009. **106**(31): p. 13010-5.

20. Ejlerskov, P., et al., *Tubulin Polymerization-promoting Protein (TPPP/p25*

alpha) Promotes Unconventional Secretion of alpha-Synuclein through Exophagy by Impairing Autophagosome-Lysosome Fusion. Journal of Biological Chemistry, 2013. **288**(24): p. 17313-17335.

21. Lee, H.J., S. Patel, and S.J. Lee, *Intravesicular localization and exocytosis of alpha-synuclein and its aggregates.* J Neurosci, 2005. **25**(25): p. 6016-24.
22. Breydo, L., J.W. Wu, and V.N. Uversky, *Alpha-synuclein misfolding and Parkinson's disease.* Biochim Biophys Acta, 2012. **1822**(2): p. 261-85.
23. Frost, B. and M.I. Diamond, *Prion-like mechanisms in neurodegenerative diseases.* Nat Rev Neurosci, 2010. **11**(3): p. 155-9.
24. Hansen, C., et al., *alpha-Synuclein propagates from mouse brain to grafted dopaminergic neurons and seeds aggregation in cultured human cells.* J Clin Invest, 2011. **121**(2): p. 715-25.
25. Braak, H., et al., *Stages in the development of Parkinson's disease-related pathology.* Cell Tissue Res, 2004. **318**(1): p. 121-34.
26. Kruger, R., T. Muller, and O. Riess, *Involvement of alpha-synuclein in Parkinson's disease and other neurodegenerative disorders.* Journal of Neural Transmission, 2000. **107**(1): p. 31-40.
27. Clayton, D.F. and J.M. George, *The synucleins: a family of proteins involved in synaptic function, plasticity, neurodegeneration and disease.* Trends Neurosci, 1998. **21**(6): p. 249-54.
28. Kahle, P.J., et al., *Structure/function of alpha-synuclein in health and disease: rational development of animal models for Parkinson's and related diseases.* J Neurochem, 2002. **82**(3): p. 449-57.
29. Mor, D.E., et al., *Dynamic structural flexibility of alpha-synuclein.* Neurobiol

Dis, 2016. **88**: p. 66-74.

30. Song, M.Y., *Role of seeded fibrillation in transcellular transmission of alpha-synuclein aggregates*. 2012, Konkuk university graduate school.

31. Conway, K.A., J.D. Harper, and P.T. Lansbury, Jr., *Fibrils formed in vitro from alpha-synuclein and two mutant forms linked to Parkinson's disease are typical amyloid.* Biochemistry, 2000. **39**(10): p. 2552-63.

32. Lee, H.J., et al., *Clearance of alpha-synuclein oligomeric intermediates via the lysosomal degradation pathway.* J Neurosci, 2004. **24**(8): p. 1888-96.

33. Lee, H.J., et al., *Formation and removal of alpha-synuclein aggregates in cells exposed to mitochondrial inhibitors.* J Biol Chem, 2002. **277**(7): p. 5411-7.

34. Langmead, B. and S.L. Salzberg, *Fast gapped-read alignment with Bowtie 2.* Nat Methods, 2012. **9**(4): p. 357-9.

35. Gentleman, R.C., et al., *Bioconductor: open software development for computational biology and bioinformatics.* Genome Biol, 2004. **5**(10): p. R80.

36. Kanehisa, M., et al., *KEGG as a reference resource for gene and protein annotation.* Nucleic Acids Research, 2016. **44**(D1): p. D457-D462.

37. Cline, M.S., et al., *Integration of biological networks and gene expression data using Cytoscape.* Nat. Protocols, 2007. **2**(10): p. 2366-2382.

38. Bae, E.J., H.J. Lee, and S.J. Lee, *Cell Models to Study Cell-to-Cell Transmission of alpha-Synuclein.* Methods Mol Biol, 2016. **1345**: p. 291-8.

39. Fischer-Colbrie, R., A. Laslop, and R. Kirchmair, *Secretogranin II: Molecular properties, regulation of biosynthesis and processing to the neuropeptide secretoneurin.* Progress in Neurobiology, 1995. **46**(1): p. 49-70.

40. Aits, S., et al., *Sensitive detection of lysosomal membrane permeabilization by*

lysosomal galectin puncta assay. Autophagy, 2015. **11**(8): p. 1408-1424.

41. Oku, Y., et al., *Synthesized Aβ42 Caused Intracellular Oxidative Damage, Leading to Cell Death, via Lysosome Rupture.* Cell Structure and Function, 2017. **42**(1): p. 71-79.

42. Aits, S., M. Jäättelä, and J. Nylandsted, *Chapter 13 - Methods for the quantification of lysosomal membrane permeabilization: A hallmark of lysosomal cell death*, in *Methods in Cell Biology*, F. Platt and N. Platt, Editors. 2015, Academic Press. p. 261-285.

43. Kissing, S., P. Saftig, and A. Haas, *Vacuolar ATPase in phago(lyso)some biology.* International Journal of Medical Microbiology, 2017.

44. Mishra, A.K., et al., *Cypermethrin Activates Autophagosome Formation Albeit Inhibits Autophagy Owing to Poor Lysosome Quality: Relevance to Parkinson's Disease.* Neurotoxicity Research, 2017.

45. Lukacs, G.L., O.D. Rotstein, and S. Grinstein, *Determinants of the phagosomal pH in macrophages. In situ assessment of vacuolar H(+)-ATPase activity, counterion conductance, and H+ "leak".* J Biol Chem, 1991. **266**(36): p. 24540-8.

46. Sacino, A.N., et al., *Brain injection of alpha-synuclein induces multiple proteinopathies, gliosis, and a neuronal injury marker.* J Neurosci, 2014. **34**(37): p. 12368-78.

47. Sacino, A.N., et al., *Intramuscular injection of alpha-synuclein induces CNS alpha-synuclein pathology and a rapid-onset motor phenotype in transgenic mice.* Proc Natl Acad Sci U S A, 2014. **111**(29): p. 10732-7.

48. Gao, H.M., et al., *Neuroinflammation and oxidation/nitration of alpha-*

synuclein linked to dopaminergic neurodegeneration. J Neurosci, 2008. **28**(30): p. 7687-98.

49. Gagne, J.J. and M.C. Power, *Anti-inflammatory drugs and risk of Parkinson disease: a meta-analysis.* Neurology, 2010. **74**(12): p. 995-1002.

50. Harms, A.S., et al., *alpha-Synuclein fibrils recruit peripheral immune cells in the rat brain prior to neurodegeneration.* Acta Neuropathol Commun, 2017. **5**(1): p. 85.

51. Sulzer, D., et al., *T cells from patients with Parkinson's disease recognize alpha-synuclein peptides.* Nature, 2017. **546**(7660): p. 656-661.

52. Hirsch, E.C. and S. Hunot, *Neuroinflammation in Parkinson's disease: a target for neuroprotection?* Lancet Neurol, 2009. **8**(4): p. 382-97.

53. Molteni, M. and C. Rossetti, *Neurodegenerative diseases: The immunological perspective.* J Neuroimmunol, 2017. **313**: p. 109-115.

54. Betarbet, R., et al., *Chronic systemic pesticide exposure reproduces features of Parkinson's disease.* Nat Neurosci, 2000. **3**(12): p. 1301-6.

55. Lin, L., et al., *Molecular Features Underlying Neurodegeneration Identified through In Vitro Modeling of Genetically Diverse Parkinson's Disease Patients.* Cell Rep, 2016. **15**(11): p. 2411-26.

56. Santpere, G., et al., *Transcriptional network analysis in frontal cortex in Lewy body diseases with focus on dementia with Lewy bodies.* Brain Pathol, 2017.

57. Mariani, E., et al., *Meta-Analysis of Parkinson's Disease Transcriptome Data Using TRAM Software: Whole Substantia Nigra Tissue and Single Dopamine Neuron Differential Gene Expression.* PLoS One, 2016. **11**(9): p. e0161567.

58. Fernandez-Santiago, R., et al., *Aberrant epigenome in iPSC-derived*

dopaminergic neurons from Parkinson's disease patients. EMBO Mol Med, 2015. **7**(12): p. 1529-46.

59. Sandor, C., et al., *Transcriptomic profiling of purified patient-derived dopamine neurons identifies convergent perturbations and therapeutics for Parkinson's disease*. Hum Mol Genet, 2017. **26**(3): p. 552-566.

국문 초록

세포 외 응집체에 의해 유도된 알파-시뉴클린 전이 매커니즘

서울대학교 대학원

의과학과

임 윤 주

알파-시뉴클린 응집체의 침적은 파킨슨병의 병리학적 특징이다. 최근 연구들에서 알파-시뉴클린 응집체의 세포 간 전이가 파킨슨병 진행의 기저를 이루는 매커니즘임을 시사하고 있다. 이 알파-시뉴클린 응집체 전이에서는 응집체가 응집과정을 촉진시키는 응집핵의 역할을 하여 전이를 증가시킨다는 '프리온-유사' 전파 가설이 있다. 그러나 이 가설은 아직 명확하게 규명된 바가 없다. 이를 바탕으로 본 연구에서는 응집핵 효과가 세포 간 알파-시뉴클린 응집체 전이에서 주요한 작용을 하는지 알아보기 위해, 응집핵 효과가 없는 돌연변이 알파-시뉴클린 V40G 응집체를 이용하였다. 그 결과, 세포 간 응집체 전이과정 증가는 응집체의 응집핵 효과에 의한 것이 아님을 확인하였다. 이는 응집체가 세포 내에서 일으키는 다른 요인 때문임을 시사한다. 추가 실험을 통해 리소좀은 손상되지 않은 상태에서 세포 외 엔도-리소좀 경로를 통한 분해 기작이 감소했음을 확인하였다. RNA 시퀀싱 분석결과, 전사조절이나 면역반응, 세포골격형성, 그리고 미토콘드리아와 관련된 유전자들이 세포 외 응집체에 의해 발현

정도가 변화했음을 확인하였다. 종합해보면, 세포 외 알파-시뉴클린 응집체는 세포 내 몇몇 매커니즘 관련 유전자들의 발현을 변화시켜 엔도-리소좀 경로를 통한 분해 기작을 감소시키고 이는 결과적으로 응집체 전이를 증가시킨다.

주제어: 파킨슨병, 세포 간 전이, 단백질 응집체, 알파-시뉴클린, 엔도-리소좀 경로, 전사체학, 유전자 발현 변화

학번: 2016-22004